universität
wien

DIPLOMARBEIT

Titel der Diplomarbeit

Design and Construction of a Monoatomic Hydrogen Beam

Verfasser

Martin Diermaier

angestrebter akademischer Grad

Magister der Naturwissenschaften (Mag. rer. nat.)

Wien, 2012

DANKSAGUNG

Abstract

One of the basic tenets in physics are symmetries. One of these symmetries the $\mathscr{CPT}$ symmetry is tested by the ASACUSA collaboration at the CERN facility. The test of $\mathscr{CPT}$ symmetry will be done in an Rabi like experiment by the ASACUSA collaboration with antihydrogen atoms, the antimatter pendent to normal hydrogen atoms. Since the creation of antihydrogen atoms is very expensive the whole setup has to be tested with hydrogen.

This thesis is about a atomic hydrogen beam setup, using a microwave discharge source for the production of a mono atomic hydrogen beam. With this source hydrogen molecules are split to hydrogen atoms in a discharge plasma by microwave radiation with a frequency of 2.45 GHz. After production the atoms escape as a hydrogen beam into a vacuum system. The setup described in this work will be the basis for the future Rabi like experiment.

Eine der wichtigsten Grundpfeiler in der Physik sind Symmetrien. Eine dieser Symmetrien, die sogenannte $\mathscr{CPT}$ Symmetrie, welche am CERN in Genf von der ASACUSA Kollaboration getestet werden soll. Diese Tests werden in einem Rabi ähnlichen Experiment von ASACUSA mit Antiwasserstoff Atomen gemacht (Antiawasserstoff ist das Antimateriependent zu Wasserstoff). Da Antiwasserstoff in der Gewinnung sehr teuer ist, sollte das gesamte Experiment auch mit Wasserstoffatomen durchgeführt werden.

Diese Diplomarbeit behandelt einen Aufbau für einen atomaren Wasserstoffstrahl und eine Quelle zur Produktion von monoatomaren Wasserstoff. Wasserstoffmoleküle werden durch Mikrowellen in einem Entladungsplasma zu Wasserstoffatomen zerteilt und dann als Wasserstoffstrahl in ein Vakuumsystem emittiert. Der Aufbau der in dieser Arbeit beschrieben wird, soll in der Zukunft die Basis für das Rabi ähnliche Experiment sein.

CONTENTS

CHAPTER 1

$\mathscr{CPT}$ PRINCIPLE

1.1 PARTICLES AND ANTIPARTICLES

The first attempt of an relativistic invariant version of the Schrödinger equation was derived of the energy-momentum equation

$$E^2 - p^2 = m^2 \qquad (c = 1) \tag{1.1}$$

where E equals total energy $E = T + m$ (p is momentum, m is mass, and T is kinetic energy). This led to the Klein-Gordon equation, which is of second order in the time derivative and has problems that the probability density is not positive definite.

Dirac wanted to derive such an relativistic invariant equation and formulated the Dirac equation for spin $1/2$ particles with mass m

$$\left(i\gamma^\mu \frac{\partial}{\partial x_\mu} - m \right) \Psi = 0 \qquad (\mu = 0, 1, 2, 3) \tag{1.2}$$

Here x_0 is the time coordinate, x_i ($i = 1, 2, 3$) are the space coordinates. This equation is of first derivative in time. γ^μ are the Dirac matrices and Ψ the spinor wave function. At the time when Dirac postulated this equation he had one problem namely that the energy eigenvalues have two solutions - positive and negative ones.

$$E = \pm\sqrt{p^2 + m^2} \tag{1.3}$$

As an interpretation of the negative solutions of his equation Dirac postulated the existence of antimatter. He meant that every particle has an antimatter pendent with same mass,

same spin, but opposite charge. 1932 Anderson experimentally discovered the existence of antimatter. He found the positron which is the antiparticle of an electron in cosmic rays. In the 1950s at the Bevatron at Berkeley the antiparticle to the proton, the antiproton - $\bar{p}$ - was found. By shooting a proton beam at a stationary target antiprotons were produced (Chamberlain et al) like [3]:

$$p + p \rightarrow p + p + p + \bar{p} \tag{1.4}$$

1.2 𝒞𝒫𝒯 SYMMETRY

In physics a symmetry means an invariant quantity under certain operation. According to Emmy Noethers theorem every symmetry yields a conservation law and also every conservation law reflects a symmetry [9]. For example the symmetry of

1. translation in time $\iff$ conservation law of energy

2. translation in space $\iff$ conservation law of momentum

3. rotation $\iff$ conservation law of angular momentum

4. gauge transformation in electrodynamics $\iff$ conservation law of charge

The fundamental symmetries in particle physics are parity transformation $\mathscr{P}$, particle-antiparticle conjugation $\mathscr{C}$ and time inversion $\mathscr{T}$.

These three operations performed together lead to one of the most important symmetries in particle physics, the so called 𝒞𝒫𝒯 invariance. As a result of Dirac's theory and the 𝒞𝒫𝒯 symmetry particles and antiparticles can be treated in the same way with the only difference that antiparticles have opposite signed charge going back in space and time.

1.2.1 PARITY $\mathscr{P}$

Parity $\mathscr{P}$ is a symmetry operation that inverts a system's space coordinates (t, x, y, z) to $(t, -x, -y, -z)$. In gravity, electro-magnetism and strong interactions this symmetry is conserved, but in weak interaction processes Parity is not conserved [15].

1956 Lee and Yang discussed Parity violation theoretical, 1957 Madame Wu had shown experimentally the broken parity conservation in Beta Decay. The result of these studies was that nearly all decay electrons are left handed (spin and momentum in opposite direction). [28, 29]

1.2.2 CHARGE CONJUGATION $\mathscr{C}$

Charge Conjugation $\mathscr{C}$ in particle physics is an operation that converts a particle into its antiparticle like

$$\mathscr{C}|p\rangle = |\bar{p}\rangle \tag{1.5}$$

$$\mathscr{C}|n\rangle = |\bar{n}\rangle \tag{1.6}$$

$\mathscr{C}$ conventionally is defined to take a fermion with a given spin orientation into an anti fermion with the same spin orientation. After it was shown that parity conservation was broken, Lee and Yang showed that charge conjugation can also not be maintained in weak interactions [15]

1.2.3 TIME REVERSAL $\mathscr{T}$

$\mathscr{T}$ like time reversal is a unitary but anti-linear operator (often called anti-unitary). It transforms a particle's time from $(t, \vec{x})$ to $(-t, \vec{x})$, This can be seen as interchanging of the forward and backward light cones [15].

1.2.4 $\mathscr{CP}$ VIOLATION

$\mathscr{CP}$ operation, the transformation of $\mathscr{C}$ and $\mathscr{P}$ at the same time, was meant to be conserved until in 1963 Cronin and Fitch observed a small violation of $\mathscr{CP}$ symmetry in the neutral Kaon system [4]. (A result of $\mathscr{CP}$ violation is the existence of three fermion families [15])

1.2.5 FROM $\mathscr{CP}$ TO $\mathscr{CPT}$

$\mathscr{CPT}$ symmetry, a combined operation of $\mathscr{C}$, $\mathscr{P}$ and $\mathscr{T}$ at the same time, is one of the most fundamental symmetries in physics. It implies that particles and antiparticles must have similar properties such as same mass and quantum numbers, the same absolute values with opposite signs of the charge like quantities and anticolors for antiquarks [5]. According to the "$\mathscr{TCP}$" theorem of Lüders and Pauli [27], it is impossible to construct a local, causal quantum field theory that violates $\mathscr{CPT}$, this violation would lead to a crisis of particle physics [16]. One way out of this crisis would be a Lorentz violating addition to the Standard Model as done by Colladay and Kostelecky [13, 14].
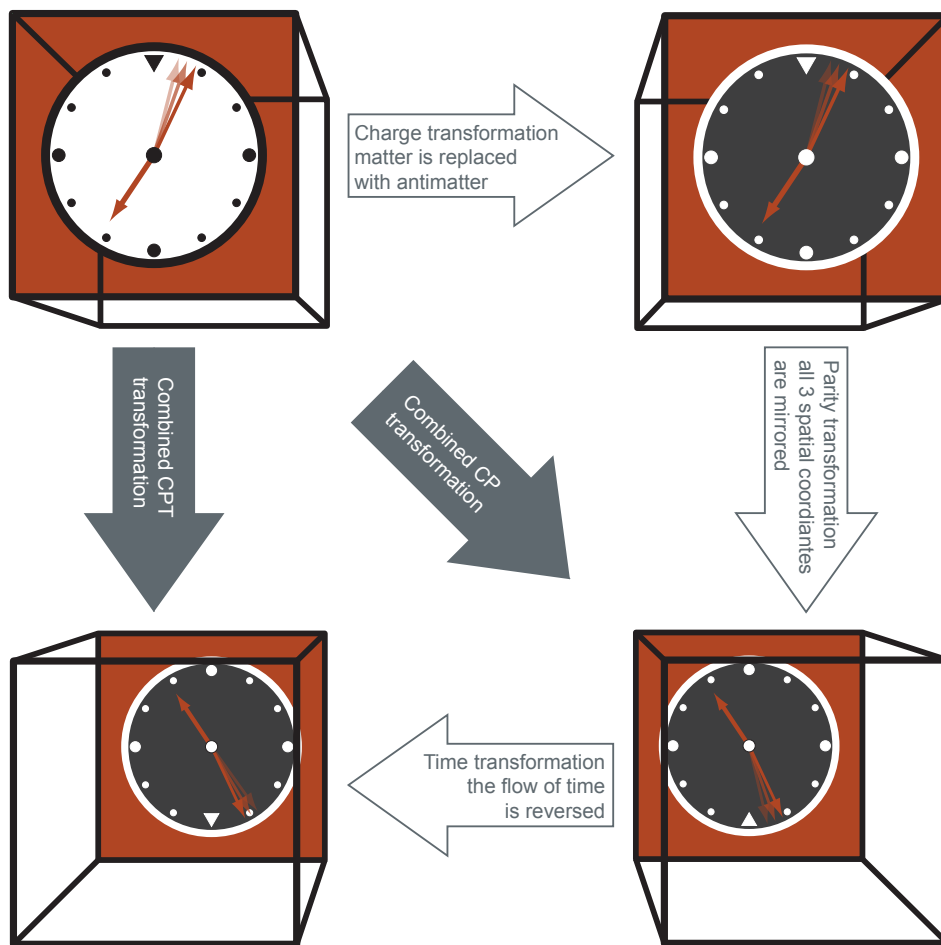
Figure 1.1: $\mathscr{C}$, $\mathscr{C}\mathscr{P}$, and $\mathscr{C}\mathscr{P}\mathscr{T}$ symmetries, (picture by Bertalan Juhasz)

If the $\mathscr{C}\mathscr{P}\mathscr{T}$ principle would be falsified, the Feynman diagram technique would lose validity. Therefore the agreement of predictions of the Standard Model should be indirect evidence of $\mathscr{C}\mathscr{P}\mathscr{T}$ invariance.

But a recent experiments of the OPERA collaboration could have shown $\mathscr{C}\mathscr{P}\mathscr{T}$ violation, since OPERA reported that they have measured a speed faster than light for neutrinos ($v_\nu \approx 1.00002\ c$) [1].

A more promising experiment to test $\mathscr{C}\mathscr{P}\mathscr{T}$ invariance is hyperfine splitting of Antihydrogen.

CHAPTER 2

ANTIHYDROGEN

Our collaboration ASACUSA (Atomic Spectroscopy And Collisions Using Slow Antipro-tons) aims to test $\mathscr{CPT}$ by doing experiments with antimatter. One of the experiments is creating antihydrogen and measure its hyperfine structure. Experiments on antihydrogen are very good to prove or disprove $\mathscr{CPT}$ principle, since the properties of the hydrogen atom, which is the matter pendent to antihydrogen, is one of the best known quantities on earth.

The hyperfine structure, which describes the splitting of the spectral lines, is a result of the interaction of the nuclear moment (proton/antiproton) with the atomic shell (electron/-positron) moment. For the hydrogen atom this quantity is very well known. Already in the 1930's, when Rabi measured the ground state hyperfine splitting (ν_{HF}) of an atomic hydrogen beam with an Stern-Gerlach like experiment (see figure 2.1). Later measurements for ν_{HF} yielded a relative precision of 10^{-12}[6].
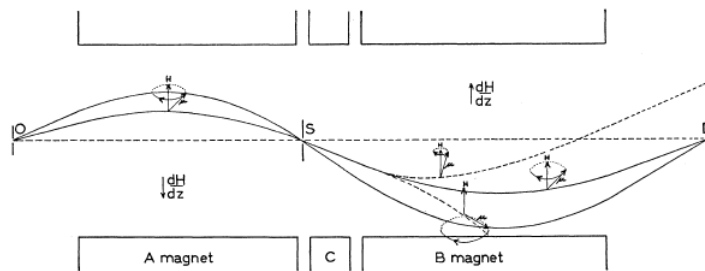

Figure 2.1: Paths of molecules in the Rabi experiment. The solid curves indicate molecules with different moments and velocities, who's moments are not changed during the passage of the apparatus. The dotted curves indicate a change of the molecules nuclear magnetic moment in the region C, these molecules therefore do not reach the detector [30].

In the hydrogen/antihydrogen atom the $1S$ ground state hyperfine structure can be

described by the interaction of the electron/positron spin $\vec{S}_e$ with the proton/antiproton spin $\vec{S}_p$ like $\vec{F} = \vec{S}_e + \vec{S}_p$, where $F = 0, 1$ is the total spin with $M_F = -1, 0, 1$ the projection of F on the magnetic field axis (see figure 2.3)[6].
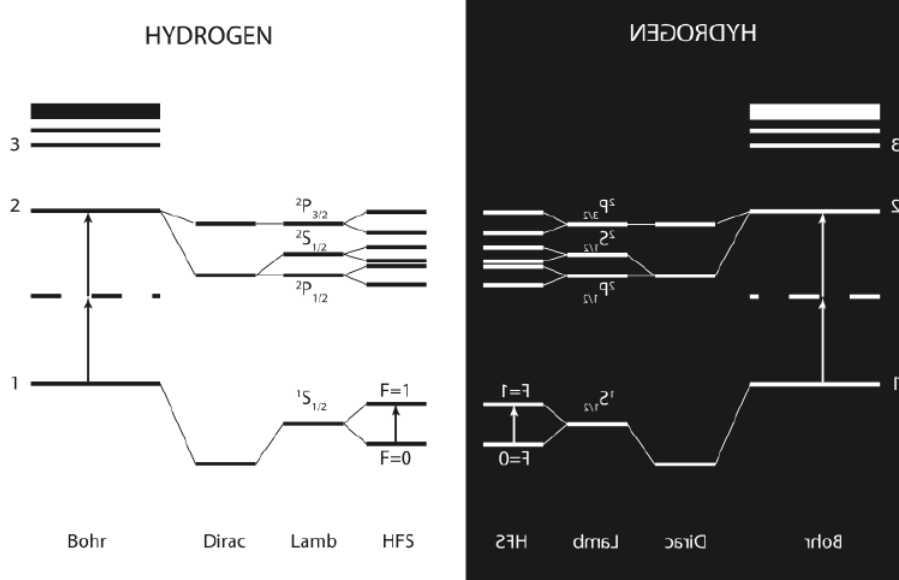

Figure 2.2: Hydrogen/Antihydrogen hyperfinestructure splitting [5].
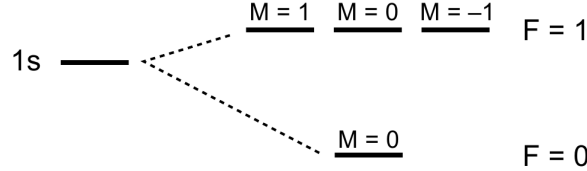

Figure 2.3: Hydrogen ground state splitting results in triplet $F = 1$ and a singlet $F = 0$ sublevels

Hyperfine splitting is directly proportional to the spin magnetic moments μ_p of the nucleus. We can describe the ground state hyperfine splitting by:

$$\nu_F = \frac{16}{3} \left(\frac{M_p}{M_p + m_e} \right)^3 \frac{m_e}{M_p} \frac{\mu_p}{\mu_N} \alpha^2 cRy \tag{2.1}$$

with the proton magnetic moment μ_p, μ_N the nuclear magneton, M_p the proton mass, m_e the electron mass, c speed of light, α the fine structure constant, Ry the Rydberg constant. This formula yields $\nu_F = 1418.84\ MHz$, which is significantly different to the experimentally value. After higher order QED corrections and non-relativistic magnetic size corrections (Zemach correction) a deviation of the theoretical value from the experimental one by

$$\frac{\nu(exp) - \nu(th)}{\nu(exp)} = 3.5 \pm 0.9\ ppm \tag{2.2}$$

was obtained.

In the ASACUSA experiment it is planned that antihydrogen atoms leave a source and pass trough

i an inhomogeneous magnetic field, to select spins and velocity

ii a microwave cavity for inducing a spin-flip transition at ν_{HF}

iii a second inhomogeneous magnetic field as analyzer of the spin flipped atoms

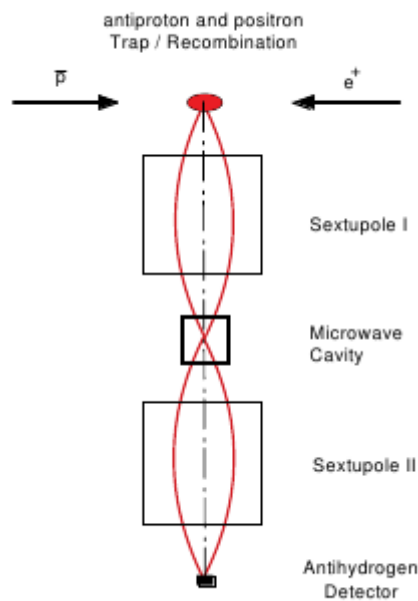(A schematic drawing can be seen in figure 2.4)

Figure 2.4: Schematic picture of a Rabi like microwave experiment for antihydrogen. Antihydrogen atoms enter the first sextupole, their trajectory gets bent, in the microwave cavity spin flip is induced, in the second sextupole magnet the spin flipped atoms are analyzed.

The magnets to be used are sextupoles. The magnetic field gradient acts on the magnetic moment of the antihydrogen atoms and therefore has, dependent on the spin-states, focusing or defocusing properties and selects spin states. Therefore, depending on the alignment of the hyperfine spin-states, the strong magnetic field will bend their trajectories. As said the four possible hyperfine states of the antihydrogen atom are $F = 0, 1$ and $M_{F=0} = 0$,

$M_{F=1} = -1, 0, 1$. These states are characterized as two pairs: the so called "high-field seekers" - they move in direction of regions with higher magnetic field, and the so called "low-field seekers", which move towards weaker field regions as seen in figure 2.5. The trajectories in figure 2.4 are low field seekers, which do not change their spin in the cavity, but if the microwave cavity would be in an resonant state the low field seekers would be transformed into high field seekers and therefore would not reach the detector. This would yield into an drop of counting rate [6].
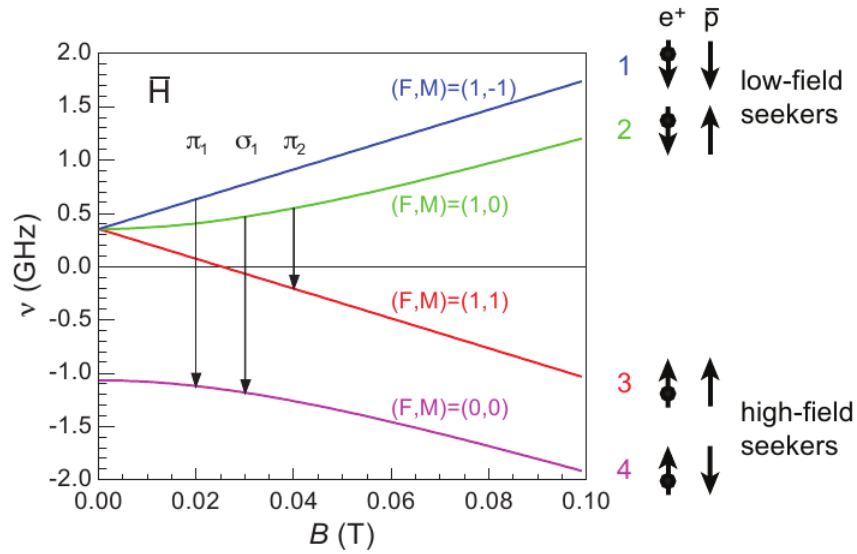

Figure 2.5: Zeeman splitting of ground state hyperfine structure levels in magnetic field. The transition from $(F, M) = (1, \pm 1) \rightarrow (0, 0)$ are called π_1, the transition from $(F, M) = (1, 0) \rightarrow (0, 0)$ is called σ_1, the transition from $(F, M) = (1, 0) \rightarrow (1, 1)$ is called π_2.

2.1 AD - ANTIPROTON DECELERATOR

The constituents of $\overline{\text{H}}$ are anitprotons and positrons. Antiprotons are produced at the Antiproton Decelerator (AD), e^+ are produced via β^+ decay, where $\text{n} \rightarrow \text{p} + \nu + e^+$.

Because antiprotonic atoms like antihydrogen require antiprotons at a kinetic energy in the eV-scale to form atoms, the antiprotons need to be cooled down after they were produced. The production is done at the PS-machine (Proton Synchrotron machine) and the cooling is done at the AD-machine which are both situated at the CERN facility close to Geneva 2.6.

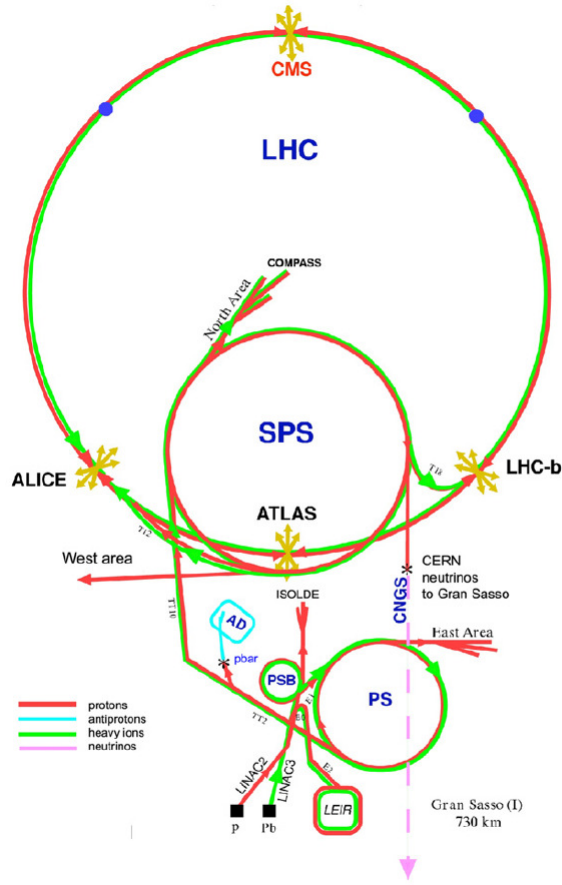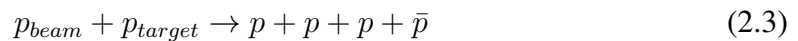The Antiprotons are produced at the PS by impinging a proton beam onto a stationary

Figure 2.6: The CERN accelerator complex. Protons are accelerated by LINAC2, PSB and then by PS. Antiprotons produced at the PS are then led to the AD, where they finally are cooled and decelerated for experiments

iridium target. The reaction forming the $\bar{p}$ beam is:

$$p_{beam} + p_{target} \rightarrow p + p + p + \bar{p} \tag{2.3}$$

Since energy has to be conserved the production energy has to be roughly above 6 proton masses $E \sim 6\,\text{GeV}$. Then an antiproton with 1 GeV rest mass will be produced. For the AD a beam of 1.5×10^{13} protons are hitting the target. Each of the protons has an kinetic energy of about 26 GeV. This energy yields to an increase of the production of antiprotons. After the reaction occurred, a $\bar{p}$ with an energy of 3 GeV emerges.

About 5×10^{7} antiprotons enter the AD with high energy and high emittance. To decrease the energy and emittance the antiproton beam has to be cooled by reducing the momentum spread. This is done via stochastic cooling, where for a subgroup of particles position and revolution frequency is measured by so called pickup coils. The signals of

the subgroups of particles are used to correct the orbit on the other side of the AD. This procedure is repeated so that the beam gets stochastically cooled and emittance reduces.
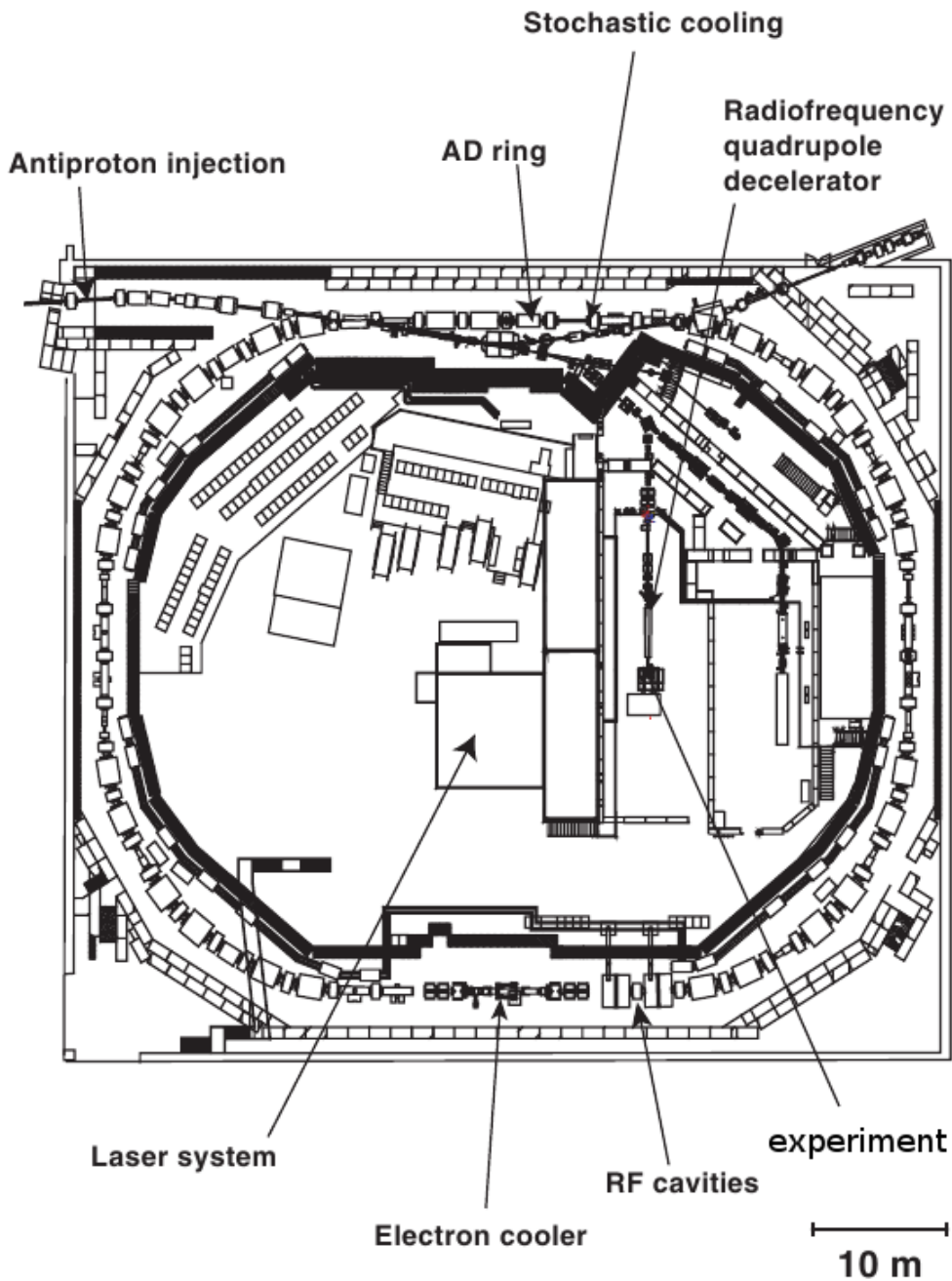

Figure 2.7: The CERN AD complex. Protons are accelerated by LINAC2, PSB and then by PS. Antiprotons produced at the PS are then led to the AD, where they finally are cooled and decelerated for experiments.

When the particles have a momentum of 300 GeV/c electron cooling is applied. The

antiprotons are merging with a stationary low temperature electron beam. Via Coulomb collision antiprotons transfer heat to the electrons which reduces momentum spread. After the 100 second cycle a 100 ns bunch of $(2 - 3) \times 10^7$ $\bar{p}$ with an energy of 5.3 MeV can be used for experiments [5].
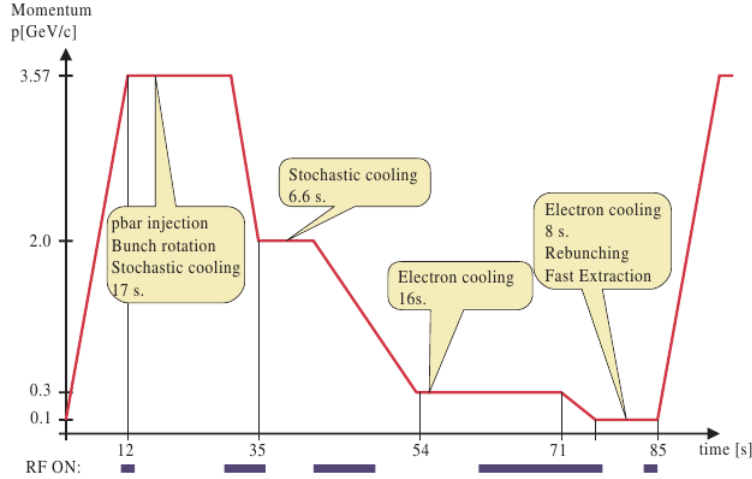

Figure 2.8: Typical AD cycle

2.2 POSITRON SOURCE

Positrons are obtained of a 50 mCi ^{22}Na radioactive e^+ source via β^+ decay.

$$p \rightarrow n + e^+ + \nu_e \tag{2.4}$$
$$^{22}\text{Na} \rightarrow^{22}\text{Ne} + e^+ + \nu_e \tag{2.5}$$

A solid moderator - frozen Ne - intercepts, cools to thermal energies and re-emits the particles. This thermalization process takes place in a few ps, while the time for annihilation takes a few 100 ps, which is the reason why this technique can be applied.

The positron then reach a differentially pumped area, where an buffer-gas is situated. Positrons slow down in the buffer-gas, in every section pressure reduces successively. A potential 'leads' the positrons in z-direction and confines them between two potential walls as seen in figure 2.9 [6, 11].
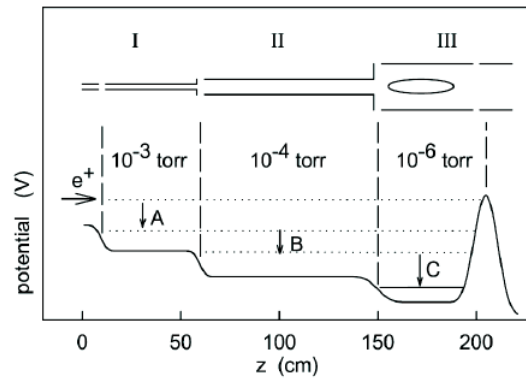
Figure 2.9: The buffer gas trap. Differential pumped sections decrease pressure. In region C positrons are confined.

2.3 RADIOFREQUENCY QUADRUPOLE DECELERATOR - RFQD

In order to further decelerate antiprotons CERN PS division and ASACUSA built an radiofrequency quadrupole decelerator (RFQD), to decelerate antiprotons from 5.3 MeV to 10-120 keV. It consists of four 3.4 m long rod electrodes. These electrodes are excited with a quadrupole RF field, where $f \sim 202.5$ MHz. The antiprotons in transverse plane are focused and defocused alternately and oscillate around the RFQD axis.

The longitudinal component of the RF field is created by the surface of the rods. A resulting standing wave along the RFQD axis is created and decelerates the antiprotons [5].
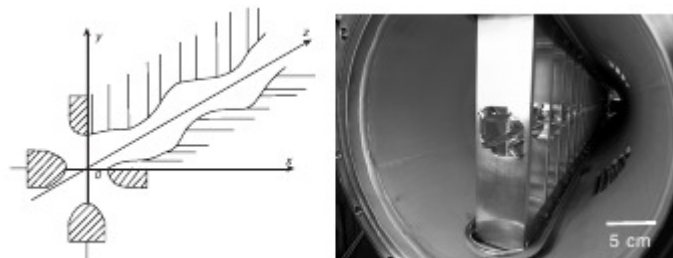

Figure 2.10: left: schematic drawing of the RFQD electrodes. right: photo of the RFQD

2.4 ANTIHYDROGEN HYPERFINE STRUCTURE EXPERIMENT

The main problem in Antihydrogen experiments is to form $1S$ ground state atoms. These atoms should be stored in neutral traps. The easiest way to form Antihydrogen atoms is a three body recombination in a high density low temperature plasma, which usually results in forming antihydrogen in high Rydberg states. But it is not possible to do spectroscopy with these high Rydberg state atoms.

In the ASACUSA experiment $\overline{H}$ are formed in an so called cusp trap, where they should be synthesized at low temperatures and stay in the trap long enough to cascade down from higher Rydberg states, where the principle quantum number is very high, to the ground state. The cusp trap consists of a magnetic quadrupole field formed by two superconducting solenoids (the cusp) and an electrostatic octupole field. An schematic view of the $\overline{H}$ setup and the cusp can be seen in figure 2.11 and 2.12.
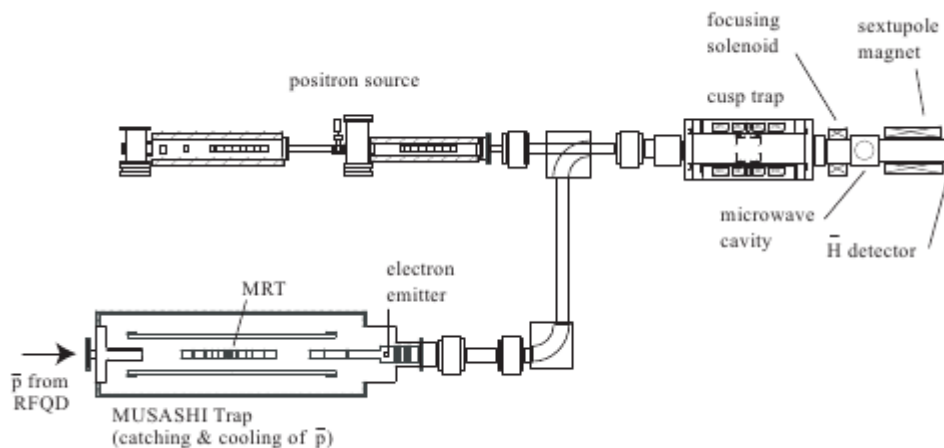

Figure 2.11: simple schematic overview the $\overline{\overline{H}}$ experiment. The cusp trap is shown together with the sextupole and $\overline{H}$ detector.

The cusp trap produces a partially spin polarized beam with low field seekers. These atoms enter the microwave cavity, where they are transformed into high field seekers via spin flip. The sextupole focuses low field seekers into the $\overline{H}$ detector and the high field seekers are defocused. Therefore if the cavity induces a spin flip, it would result in a drop of the counting rate at the detector [6].
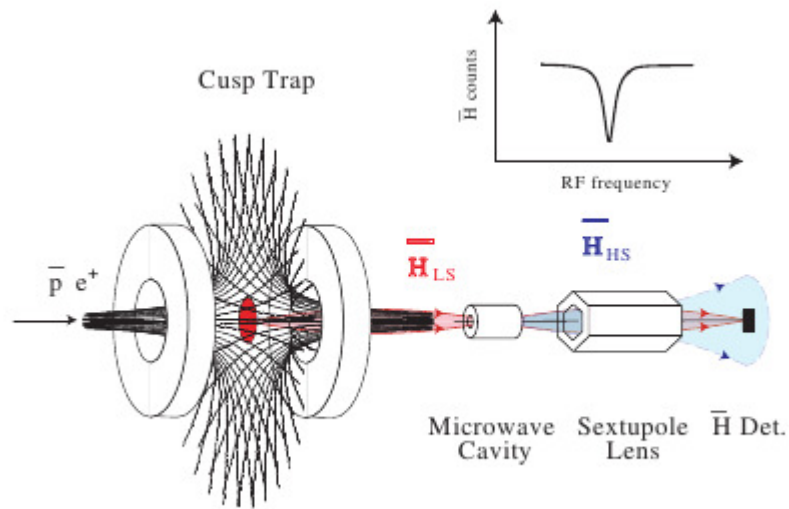
Figure 2.12: simple schematic overview the $\overline{\mathrm{H}}$ experiment. The cusp trap is shown together with the sextupole and $\overline{\mathrm{H}}$ detector.

2.5 HYDROGEN EXPERIMENT

Compared to the production of antihydrogen the production of monoatomic hydrogen is very cheap. The whole setup of the ASACUSA experiment with sextupoles in Rabi configuration has to be tested and understood. Therefore in the near future it is planned to perform the ground state hyperfine structure experiment with normal hydrogen atoms.

My work for this antihydrogen/hydrogen experiment was to design and study a source for the production of monoatomic hydrogen, build a setup for a hydrogen beam in a vacuum system and improve the detection for such a beam.

CHAPTER 3

HYDROGEN FORMATION COOKBOOK

3.1 COLLISION PROCESSES IN A DISCHARGE PLASMA

The source for production of a hydrogen beam is a glass discharge tube, where a hydrogen plasma is maintained by 2.45 GHz microwave radiation.

There are few processes how to produce atomic hydrogen in a plasma. In principle one can say that molecular ionization/dissociation has to compete with an ionization process. "Because of the distribution of electron energies, the rate at which any reaction proceeds depends on the onset energy and the cross section immediately beyond onset much more sensitively than on the maximum cross section."[26] As can be seen in table 3.1 reaction 2 and 3 can be neglected because of too high onset energy. The atomic hydrogen is mainly produced by a two stage process.

The reactions that are formed by two stage process are reaction 4, 5 and 6 and since the density of molecular ions is much smaller than that of molecules the dominant process is reaction number 5. Also the other processes are not really important, because there are not enough excited reaction partners.

The rate P, at which different processes occur with different electron temperatures is given as

$$P = nn_eQ \tag{3.1}$$

No.	Process	Onset (eV)	σ_{max} $(10^{-16}cm^2)$	E at σ_{max} (eV)
1	$H_2 + e \rightarrow H_2^+ + 2e^-$	15.4	1.1	80
2	$H_2 + e \rightarrow H^+ + H + 2e^-$	18.0	0.005	120
3	$H_2 + e \rightarrow H^+ + H^+ + 3e^-$	46	0.005	120
4	$H_2^+ + e \rightarrow H^+ + H + e^-$	12.4	3-16	16
5	$H_2 + e \rightarrow H + H + e^-$	$\simeq 8.5$	0.6	12
6	$H_2^+ + e \rightarrow H + H$	0	100(?)	-
7	$H + e \rightarrow H^+ + 2e^-$	13.5	0.65	40
8	$H + e \rightarrow H^*(2P) + e^-$	10.2	0.7	25
9	$H^* + e \rightarrow H^+ + 2e^-$	3.3	15	9
10	$H_2 + e \rightarrow H_2^* + e^-$	10.3	0.2	60
11	$H_2^+ + H_2 \leftrightarrow H_3^+ + H$	thermal	large	-

Table 3.1: Onset energy of electrons, maximum cross section σ_{max} for various processes and its corresponding energy E

with n = number of atoms/molecules, n_e electron number density and the raction parameter Q [cm^{-3}s^{-1}] as

$$Q = \int_0^\infty \sigma(E) \left(\frac{2E}{m}\right)^{\frac{1}{2}} f(E)dE \qquad (3.2)$$

$f(E)$ is assumed to be a Maxwellian energy distribution. Values for Q are given in table 3.2 with mean energies $\overline{E} = 3k_eT/2 = 4, 6, 8$, and 10 eV [25]

$\overline{E}$	$H_2 \rightarrow H_2^+$	$H_2 \rightarrow H + H$	$H \rightarrow H^+$	$H \rightarrow H^*(2P)$	$H^* \rightarrow H^+$
4	3.1	29	5.9	48	5×10^3
6	31	95	40	150	10^4
8	95	170	110	300	10^4
10	200	220	210	470	10^4

Table 3.2: Q values, in units 10^{-11}cm^{-3}sec^{-1} and unit number density nn_e

3.2 RECOMBINATION EFFECTS

At room temperature and a pressure where the atomic beam is formed (<1 mbar) recombination effects are quite important factors, since they can decrease the amount of hydrogen atoms very drastically. Principal loss mechanisms are first-order wall effects, according to Walraven and Silvera volume recombination is negligible [21]. Thus it can be suggested

that the atoms hit the wall and with a certain probability can recombine to a molecule, which will leave the orifice of the glass tube. The second constituent of the recombination process can be a residual impurity that already stuck on the wall or can also be an atom, molecule from the plasma.

The recombination process can be described by a recombination coefficient γ for different materials where the atoms strike against the wall. The containment of the hydrogen gas therefore should have a small recombination coefficient. Donnelly et al. said that the best materials known are clean Pyrex, quartz and PTFE (Dupont Teflon 120 FEP), which was the reason why the discharge tube was built of Pyrex [19, 23]. (For example the recombination coefficient for $\gamma_{Teflon} = 2.1 \times 10^{-5}$ and $\gamma_{Pyrex} = 4 \times 10^{-3}$). For deeper understanding of recombination of atoms one can read the very detailed works [21] or [23].

3.3 DETERMINATION OF THE PLASMA TEMPERATURE

For a Maxwellian electron energy distribution in the plasma and a mean free path λ_e for elastic scattering less than r the radius of the tube, "Schottky's theory of positive columns" can be used to describe the plasma temperature.

$$\frac{R^+(kT)}{kT} = \frac{1}{(dp_s r)^2} \tag{3.3}$$

$R^+(kT)$ is the rate coefficient for ion production at an electron temperature kT in [eV], p_s the pressure of gas in the discharge tube and d a constant related to the diffusion constant. This formula allows to estimate the electron Temperature as a function of pressure in the tube. For low pressures, where $\lambda_e > r$ von Engel gave the expression

$$kT = 13.6/ln(641ap_a) \tag{3.4}$$

(p_a is the atom pressure, a a constant expressed in number of ion pairs [cm^{-1}Torr^{-1}V^{-1}] at the electron ionization threshold). A plot of the two equations has been done by Geddes et al. to show electron temperature (see figure 3.1) [26]
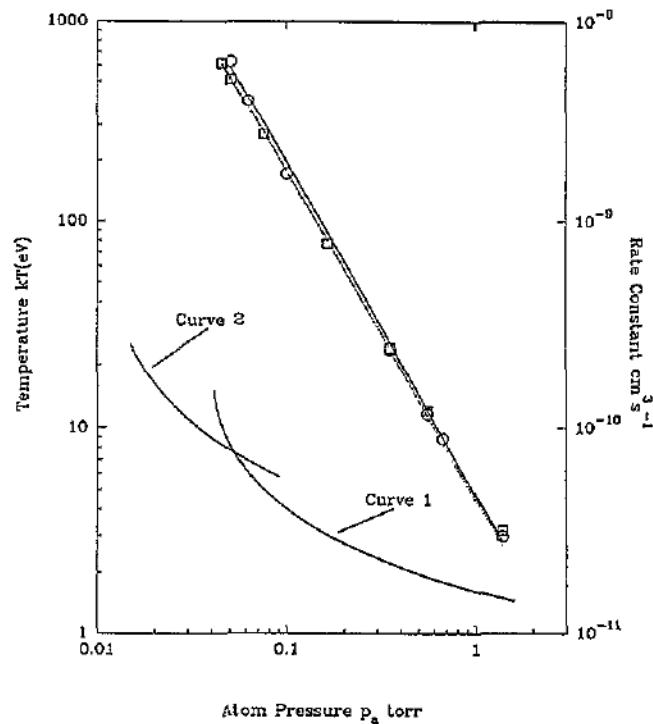
Figure 3.1: electron atom pressure vs. temperature (left) and rate constant (right) curve 1: using equation 3.3 for $\lambda_e < r$, source pressure = atomic pressure, $d = 7.2 \times 10^5$ (from Goodyear and von Engel) curve 2: using equation 3.4 for $\lambda_e > r$ line: measurements they have done for $e + H \to H(n = 2) + e$ (circles) and $e + H_2 \to H + H + e$ (squares).

3.4 SLOT ANTENNA

In many applications in physics the production of hydrogen atoms is done by microwave discharges which produce a plasma out of hydrogen molecular gas. Usually hydrogen molecules gas is led into a cylindrical tube made of glass, where the microwaves create the plasma. At the end of the glass tube hydrogen atoms leave through a small nozzle like capillary.

One commonly used type of source is the so called Lisitano-type. The Lisitano coil consists of a slotted metal cylinder surrounding the glass tube like in 3.2. This slotted line antenna has a quite homogenous and efficient power transfer to the plasma, its field distribution is approximately like a TE_{0j} (electrical vector perpendicular to propagation, for more detail see appendix) mode in a cylindrical cavity where $j = 0, 1, ...$
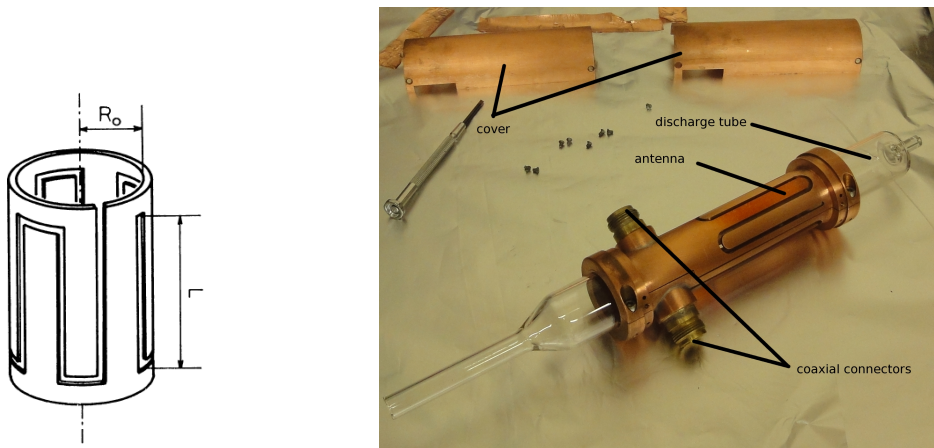
Figure 3.2: left: schematic drawing of the antenna of a Lisitano coil [20]; right: picture of the our discharge source.

3.5 THE SOURCE

Microwaves with a frequency of 2.45 GHz are produced by a 300 W microwave generator. The microwaves are led through a microwave cable, N type coaxial connectors to the Lisitano coil. The connectors are fed through a 1.5 mm thick cylinder made of copper and then lead the microwaves to the resonator. The resonator consists of coupling slots (antennas) where every slot is the half of the wavelength of the microwaves $\lambda/2$ long. The Lisitano coil can be seen as a system of N slot antennas, distributed uniformly over a cylinder, which all are radiating in phase. When microwaves are led into the resonator standing wave nodes of the electric field are at the position of the coupling slots. In the vacuum the electric fields of the slots interfere constructively and a TE_{0j} (for theoretical aspects about TE_{0j} see in the appendix) field in plasma direction similar to a cavity is formed [17, 20] (A schematic drawing of the intensity of the E field for a slot antenna can be seen in figure 3.3).

The B field can be neglected, since it does not transfer a big amount of energy to the system. The discharge of the plasma can be started by using a 240 V spark from a Goodburn Engeneering tesla coil onto the glass tube, when microwaves are turned on.

The discharge tube was mounted on a flange and the output of the source pointed direct into a vacuum chamber. The source was water cooled by small water conduits through the mounting of the discharge tube. As said the atoms exited directly through the small capillary into the vacuum. This small capillary made a big pressure difference possible. Depending on the gas flow the pressure in the vacuum chamber direct after the capillary usually was $10^{-6} - 10^{-7}$ mbar, while the pressure in the source was in the order of $\sim 10^{-1}$
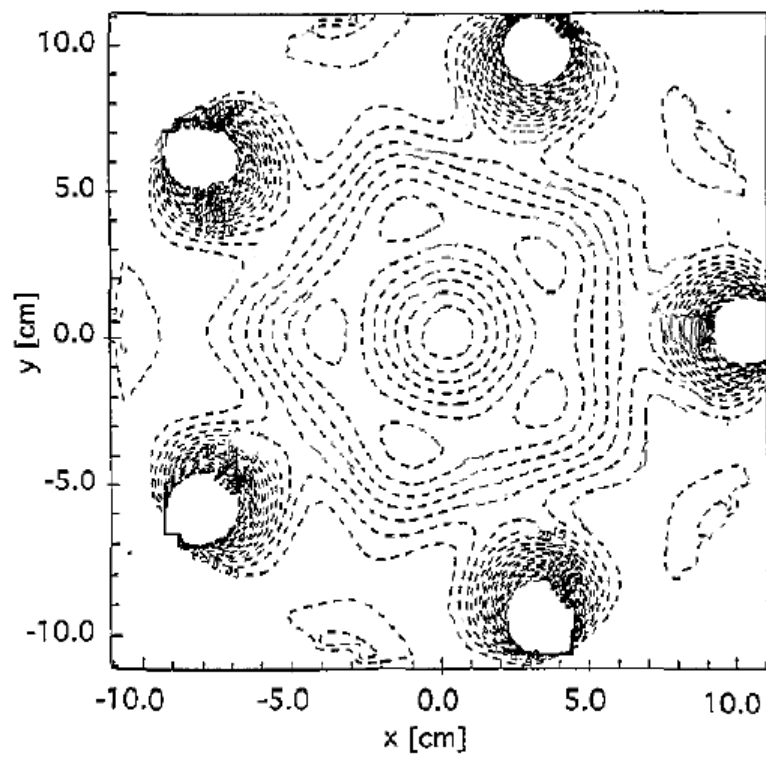
Figure 3.3: schematic drawing of the intensity $|E|^2$ of the E field for a slot antenna with 5 antennas by Werner et al. [17]

mbar.
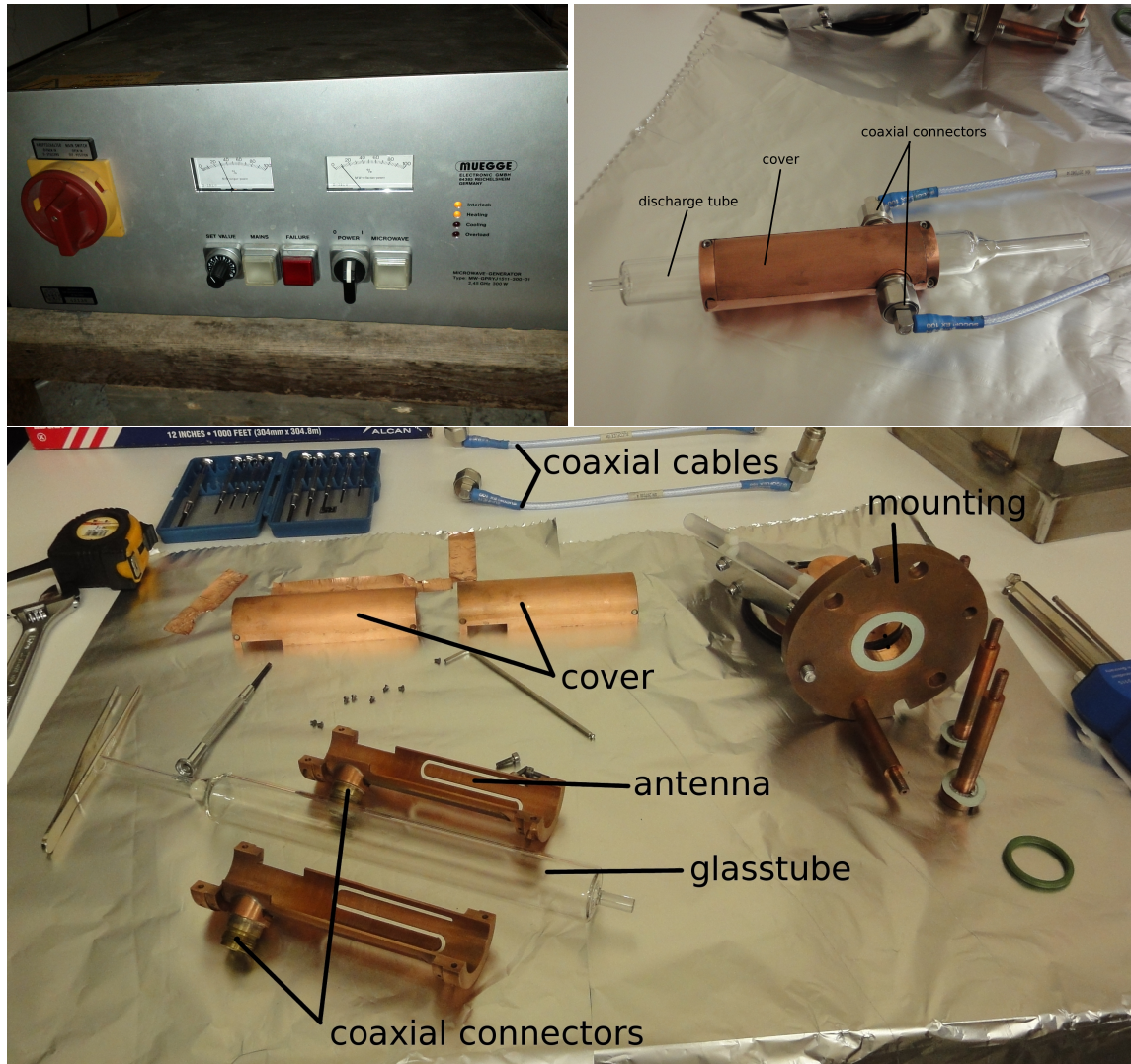
Figure 3.4: left upper corner: the microwave generator; right upper corner: a glass tube, where the microwaves are radiated into; bottom: the Lisitano coil segmented. On the bottom of the picture the antennas, made of copper can be seen.
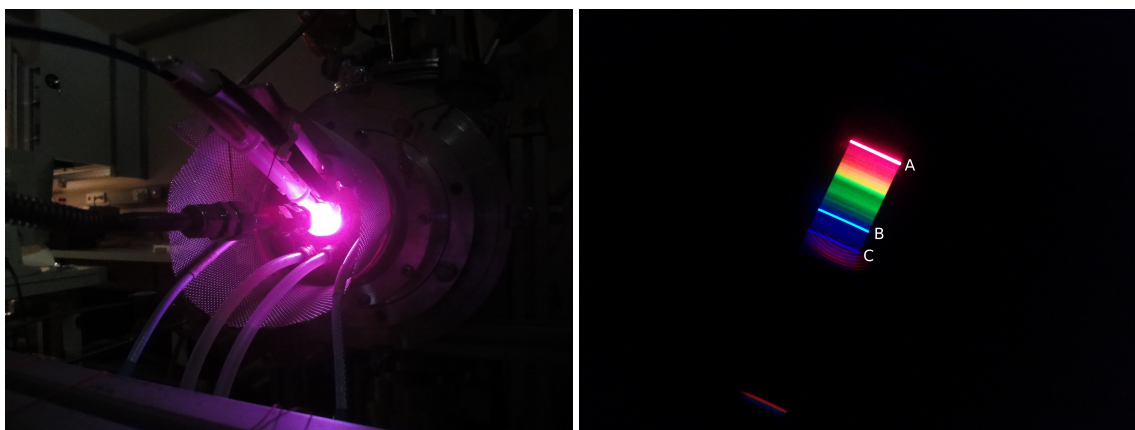
Figure 3.5: left: The red-pink color coming from the Balmer series; right: The Balmer lines of the atomic hydrogen plasma seen by a hand spectrometer. A: H-α spectral line ($n: 3 \rightarrow 2$), B: H-β spectral line ($n: 4 \rightarrow 2$), C: H-γ spectral line ($n: 4 \rightarrow 2$).

When ignited the plasma has a red-pink color, which comes form the atomic Balmer series like:

$$\lambda = G \frac{n_1^2}{n_1^2 - 4} \tag{3.5}$$

for n_1 = 3,4..., G is an empirical constant ($G = 3.645 \times 10^{-7}$ m) [8].

3.5.1 CHARACTERISATION OF THE PYREX TUBE

The pyrex tube for the dissociation of molecular hydrogen was characterized by the reflected microwave power back into the microwave power supply. Plots of the pressure of the hydrogen gas supply vs. the reflected microwave power can be seen in figure 3.6 and 3.7 (the reflected microwave power was displayed at the analog readout of the microwave generator). The plot shows the best working points for 30% an 40% microwave power, where the plasma absorbs most of the power.

3.5.2 CLEANING OF THE SOURCE

After various tests it can occur, that the glass tubes become dirty, but for an effective dissociation of hydrogen the surface has to be very clean.

Koch and Steffens described how to clean the surface of the pyrex tubes. A very good solution is first to clean the tube with acetone, methanol and distilled water, then give them into a 2:1 acid mixture of concentrated hydrofluoric acid HF(40%) and hydrochloric acid HCL(32%) for approximately 5 minutes, cleaning with distilled water again and finally

baking it out in a vacuum for 24 hours at $150°$C [12].
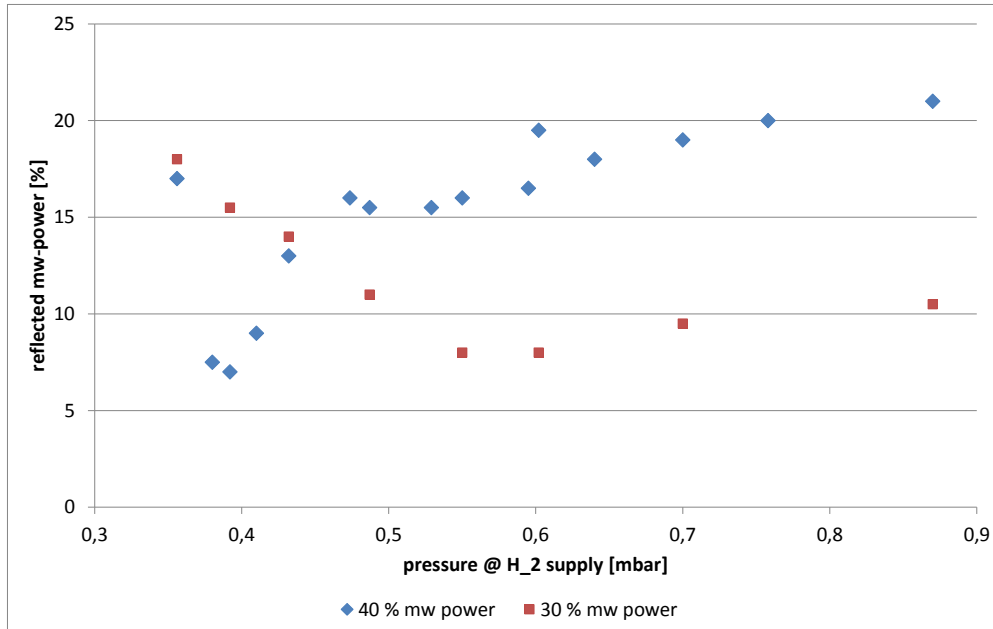
Figure 3.6: Reflected microwave power (for 30% and 40% mw power) as a function of the pressure in the H_2 supply. The graph shows, that the best working points for different microwave power coming from the power supply. For 30% microwave power the best working point is around 0.6 mbar at the gas supply and for 40% microwave power the best working point is around 0.4 mbar pressure at the gas supply.
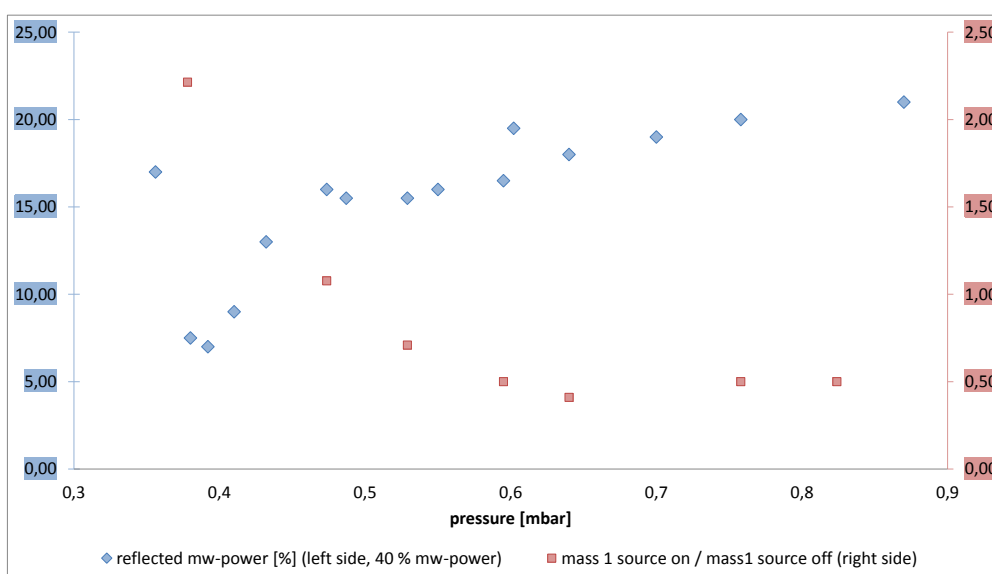
Figure 3.7: Reflected microwave power for 40% microwave power as a function of the pressure in the H_2 supply. The graph shows, that the best working point is around 0.4 mbar. If gas pressure at the hydrogen supply is lower than 0.4 mbar reflected microwave power rises again, because there is not enough gas to absorb the microwaves. A lower gas H_2 supply would maybe damage the source. It can also be seen that the ratio of the partial pressures of atomic hydrogen - when source is turned on vs. when source is turned off - is higher around this working point.

CHAPTER 4

EXPERIMENTS

4.1 TESTING NOZZLES

The first experiment was the measurement of a gas beam, which was shot through a nozzle in a vacuum system, because we wanted to get a feeling for different types of nozzles. Thus we scanned the beam with a pressure gauge (Leybold Ceravac CTR90) connected to a pitot tube. The pitot part mounted on a in xyz-direction moveable frame was moved by small bi-step motors. The motors were navigated by a LabView program via a RS232 COM port (The program can bee seen in the appendix).
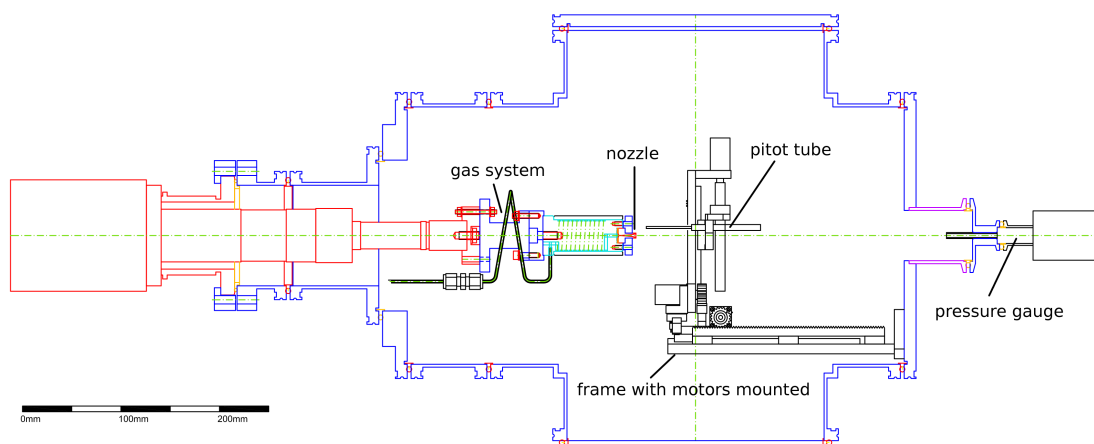
Figure 4.1: Setup of the vacuum chamber with the pitot tube

The vacuum system consisted of a backing pump (Leybold TRIVAC B S65B) and a roots pump (Leybold RUVAC WAU 501). With this vacuum system a pressure in the region of 10^{-3} mbar was reached. A schematic setup is shown in figure 4.1.

Different gases such as Ar, He, Air, were led through a nozzle (diameter $60\ \mu$m). A flowmeter (OMEGA FMA-1904-N2) adjusted the gas throughput, adjustable from 0-20 standard cubic centimeter per minute (sccm). An air filter, mounted after the flowmeter, made shure that the nozzle was not plugged by dust.

In the first test no nozzle was used. A profile of this gas jet can be seen at figure 4.2.
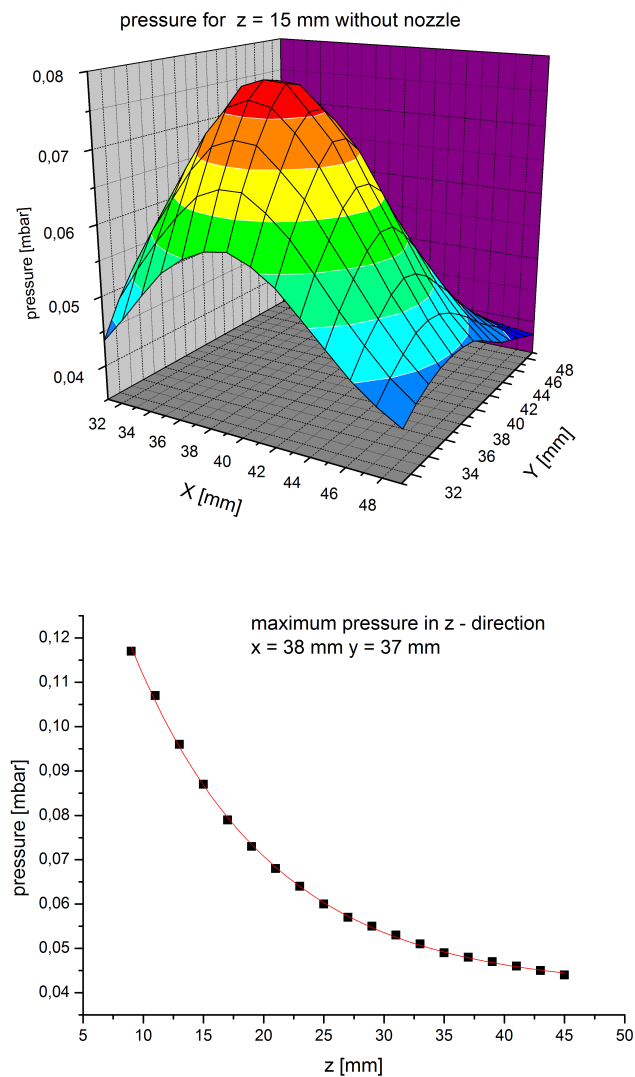
Figure 4.2: Scan of the air gas jet, 15 sccm gas flow, no nozzle, the second plot was fitted with an exponential decay.

The next test was done with a laval type nozzle with a diameter of $40\ \mu$m. The geometri-

cal form of the nozzle was similar to figure 4.3.
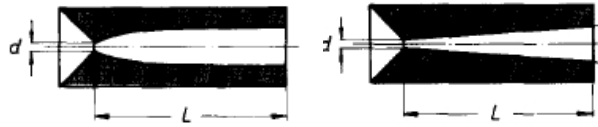
Figure 4.3: left: laval type nozzle; right: conical type nozzle [22]

Figure 4.4 shows tests, which were done with helium as gas jet. The pressure intensity decays exponentially in z direction.
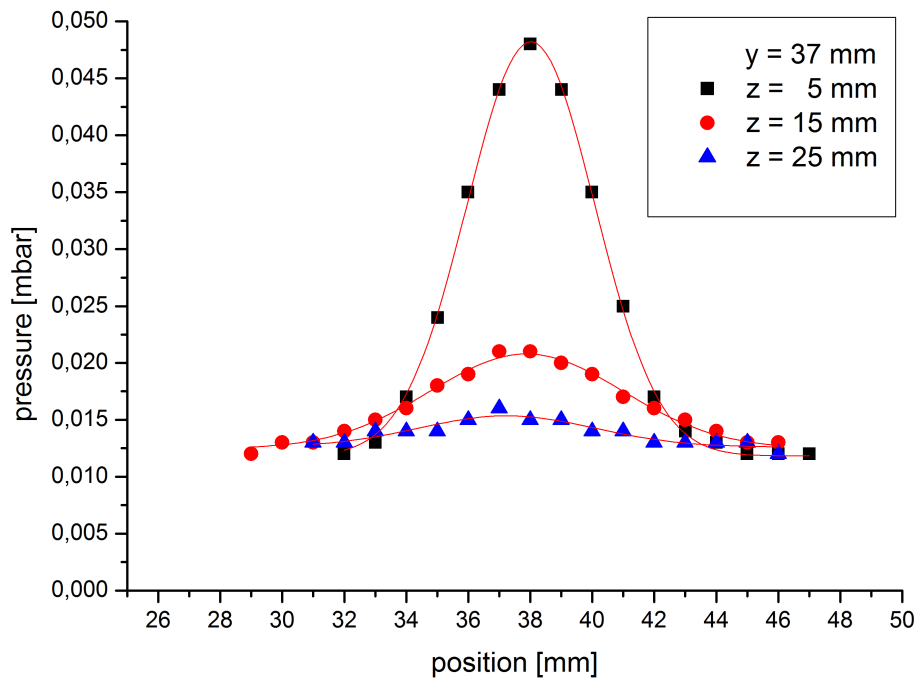
Figure 4.4: He tests with nozzle, 15 sccm. The pressure profile is fitted with a gaussian function. (FWHM for: Fit 1 (z = 5 mm): 4.93 mm; Fit 2 (z = 15 mm): 7.33 mm; Fit 3 (z = 25 mm): 6.67 mm)

A defect of the pumping system made a change of the vacuum pumps necessary. A backing pump Varian OME SD 700/1400 and a turbo molecular pump (TMP) Leybold Turbovac 361 with a control unit TURBOTRONIC NT20 were used. The TMP was water cooled. With this pumping system a base pressure of about 2×10^{-6} mbar was attained. After opening the valve at the flow meter with a gas flow of 15 sccm pressure increased to 4.6×10^{-4} mbar.

In the next step a new nozzle built by our workshop was tested. The diameter was $500 \ \mu$m and it had a conical form.

The results are shown in fig. 4.5 and fig. 4.6. In a distance of 50 mm the pressure gauge was not able to distinguish between jet and background. Also measurements with 20 sccm were done but the result was approximately the same. The pressure profile of the nozzle made by our workshop has a Lorentzian shape. By comparison the shape of the laval nozzle has a gaussian form.
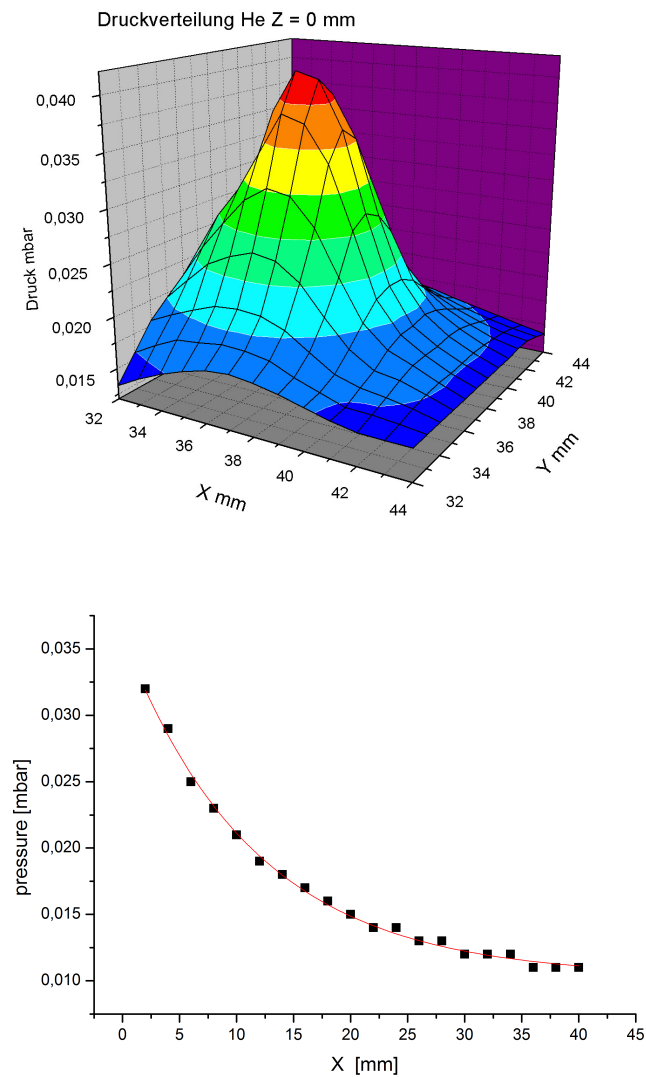
Figure 4.5: He tests with conical nozzle, 15 sccm, the second plot was fitted with an exponential decay.

An additional data set was measured with Argon. At 10 sccm gas flow the pressure rises in the vacuum chamber from 2×10^{-6} mbar to 2×10^{-3} mbar, with a gas flow of 15 sccm
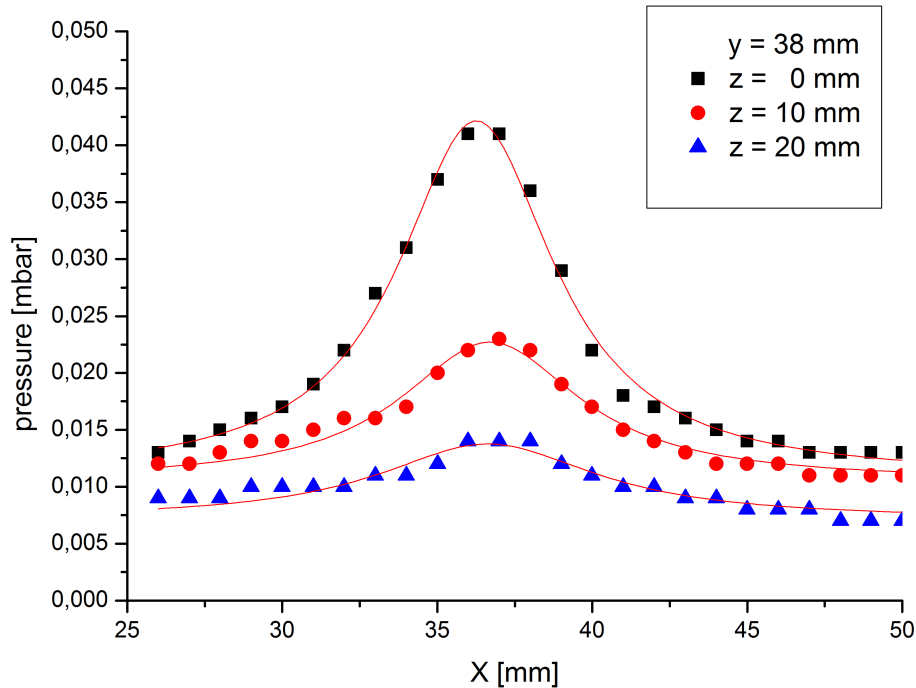
Figure 4.6: He tests with conical nozzle, 15 sccm. The pressure profile in the is fitted with a lorentzian function. (FWHM for: Fit 1 (z = 0 mm): 7,24 mm; Fit 2 (z = 10 mm): 8,29 mm; Fit 3 (z = 20 mm): 10,17 mm)

the pressure rises to 2.4×10^{-3} mbar.

The results of this first experiment was, that the nozzle form has an effect on the shape of the pressure distribution. While the laval type nozzle, which had a rather small diameter (diameter 40 μm), formed a gaussian distributed pressure profile, the second nozzle (conical one, diameter 500 μm) had a Lorentzian pressure profile. But it can also be seen that the diameter of the nozzle does not disturb the maximum pressure intensity drastically. Further it can be seen that the pressure signal decays exponentially with the distance, which means that the beam diverges. As a conclusion of this experiment we could see, that there was not a need of a special nozzle geometry and also that with a diameter of 500 μm the pressure profile was acceptable for our purpose. Since for $z > 10$ mm we had a very broad distribution of the pressure profile, we concluded that the placement of the skimmer and the blends was not necessary to be tuned extremely fine in the following setups.
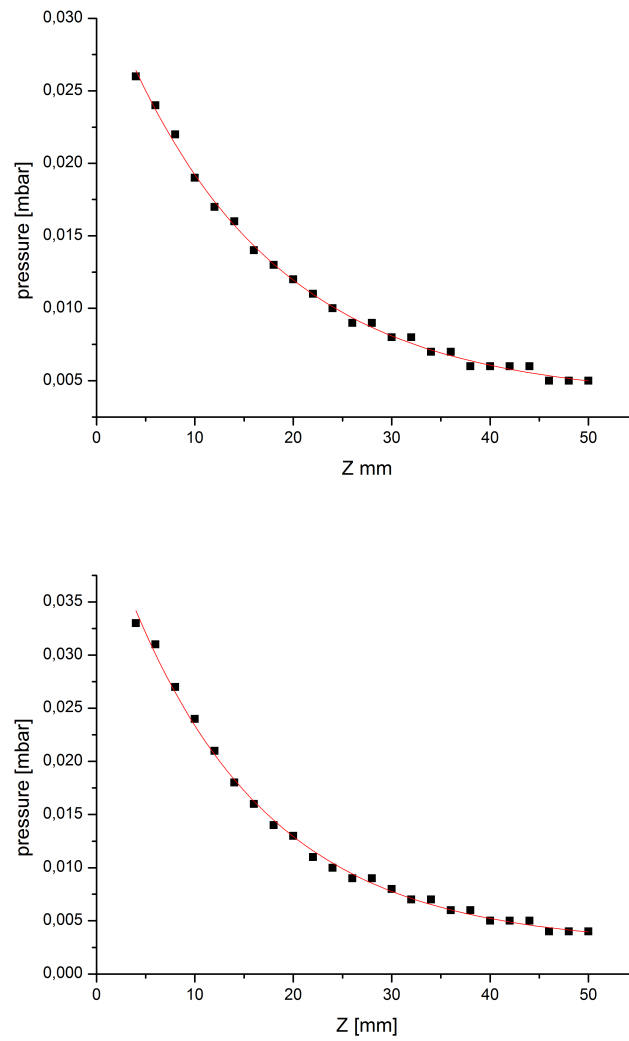
Figure 4.7: Ar tests with conical nozzle in z direction, first: 10 sccm, second: 15 sccm gas flow, the plots were fitted with an exponential decay.
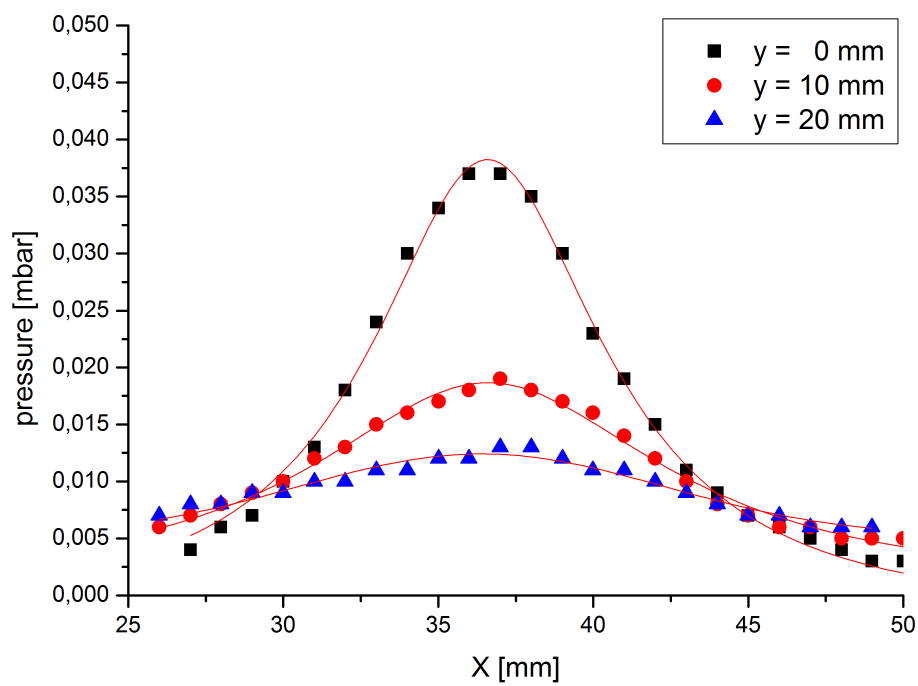
Figure 4.8: Ar tests with conical nozzle, 15 sccm gas flow. The pressure profile in the right plot is fitted with a lorentzian function. (FWHM for: Fit 1 (z = 0 mm): 6,94 mm; Fit 2 (z = 10 mm): 10,77 mm; Fit 3 (z = 20 mm): 16,45 mm)

4.2 ATOMIC BEAM SETUP

In order to have a good signal to noise ratio of the atomic hydrogen beam signal, an excellent vacuum had to be created. To do so the atomic beam was shot through differentially pumped vacuum chambers through small slits (see figure 4.12).

4.2.1 GAS SYSTEM

The dissociation source needed hydrogen molecules for the production of hydrogen atoms. A tank filled with hydrogen served as a reservoir. Pressure gauges measured the pressure of the tank (Keller AG 23 0-20 bar) and the supply pipes (Keller AG PAA-21-10). Furthermore a diaphragm pump (Pfeiffer MVP 055-3) evacuated the whole gas system before usage of hydrogen to make sure that only clean gas reached the hydrogen dissociation source. A schematic drawing of the whole gas system can be seen in figure 4.9.
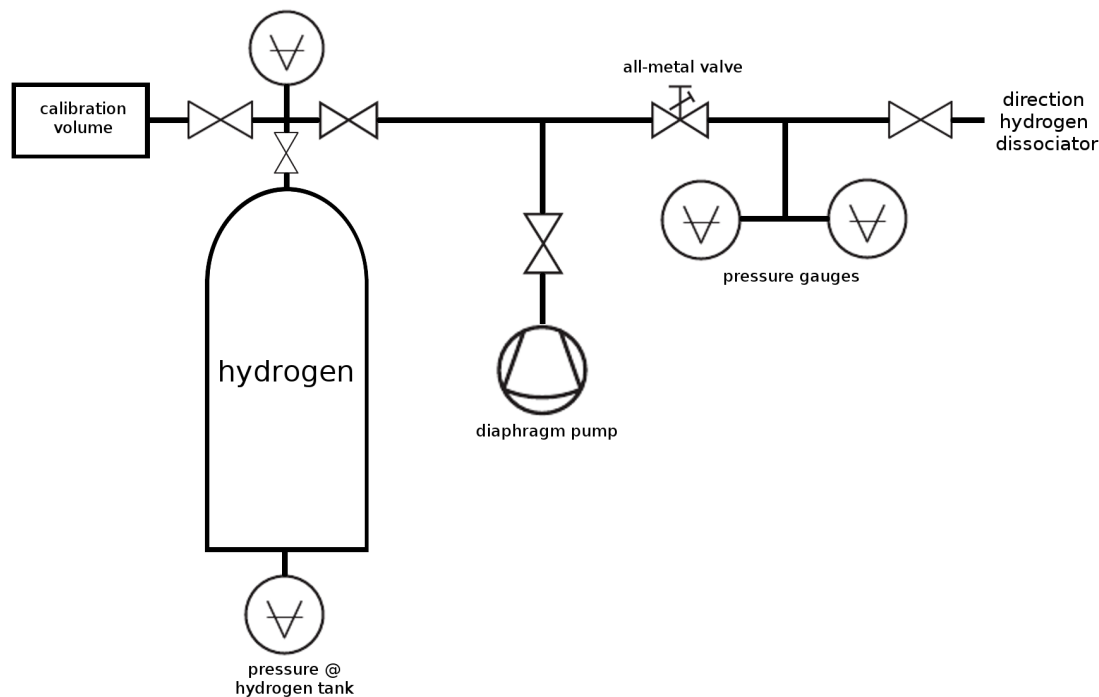
Figure 4.9: Schematic drawing of the Gassystem.

The hydrogen gas went from the gas tank through a all-metal UHV inlet valve (Balzer UDV 040), which reduced the pressure and adjusted the gas flow in the glass tube side. Direct after the inlet valve two pressure gauges were also mounted (Leybold CTR 90, A-Net Crystal gauge). With a calibration volume ($30 \ cm^3$) the gas flow could be measured.
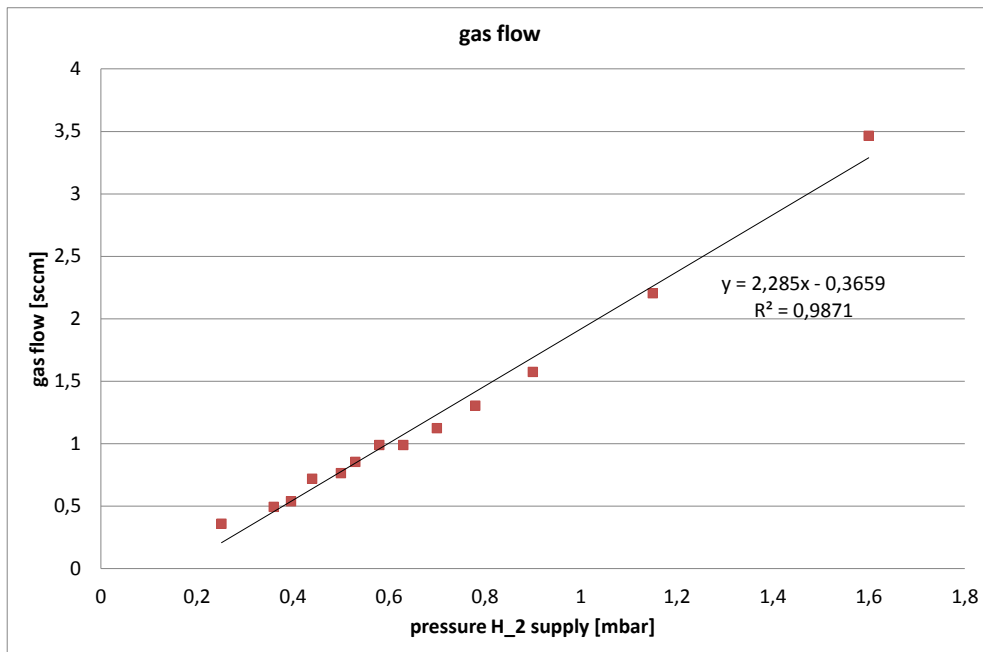
Figure 4.10: The gas flow through the system as a function of H_2 supply.

This could be done as follows: With the calibration volume the volume of the pipes could be estimated. When the all-metal valve was opened, pressure in the tubes decreased. With the pressure difference after one minute opened and the ideal gas equation ($pV = const.$) the gas flow could be calculated.

In the tank there was a pressure of some bar, which was reduced by the inlet valve so that in the source the maximum pressure was in the order of one millibar.

GAS FLOW

As said the gas flow was simply calculated by the usage of a calibration volume. With a known pressure in the calibration volume one could estimate the volume of the tubes leading to the inlet valve (the big hydrogen reservoir was closed, only a small amount of gas was in the gas system). When the inlet valve was opened the pressure in the tubes slowly reduced over time. With this measurement a correlation between pressure at the source and gas flow could be computed.

4.2.2 NOZZLE, BEAM FORMATION

A first collimation and formation of the beam emerging from the capillary was done by a nozzle (in some experiments the beam was formed without nozzle, which meant that the capillary alone formed the beam. The small diameter of the capillay also had a kind of nozzle effect). Afterward slits and one skimmer formed the beam in three differentially pumped vacuum chambers, each having a better vacuum. In the last chamber a quadrupole mass spectrometer detected and analyzed the beam. The whole setup can be seen in figure 4.12.

The skimmer is a conical object with a hole in the middle, which skims a gas beam and thus brings collimation. Only the intense central component of the gas jet will reach the next differentially pumped area. The diverging part of the beam will not reach the next chamber, after the skimmer only the directed beam component is present.

It is assumed, that when entering a skimmer the gas has a Maxwell distribution for the velocities. Thus the velocity distribution of atoms and molecules in the beam could be given as

Figure 4.11: schematic drawing of a skimmer [10]

$$\frac{dI_0}{dv} = A_s n_s \frac{1}{\pi l^2} \frac{1}{\pi^{\frac{1}{2}}} \left(\frac{m}{2kT_s} \right)^{\frac{3}{2}} v^3 e^{-\frac{m}{2kT_s}(v-v_s)^2} \tag{4.1}$$

with T_s the temperature of the gas stream, dI_0 the intensity of molecules and atoms in the velocity interval dv, A_s the skimmer entrance area, n_s the number density of atoms molecules at the skimmer entrance, l the distance downstream at the skimmer entrance, m the molecular or atomic mass, k the Boltzmann constant and v_s the gas stream velocity. Since the properties of our gas beam was a subsonic gas jet the density distribution should be quite broad [24]

4.2.3 QMS DETECTION SYSTEM

In this first assembly the rest gas was analyzed with a quadrupole mass spectrometer. The used QMS was made by Spectra with a faraday cup and a secondary electron multiplier (SEM). The QMS was calibrated with helium and argon gas, which was introduced through a inlet valve (Balzers UDV 040) at the last chamber. When pressure reached the 10^{-8} mbar region the SEM of the mass spectrometer was used instead of the faraday cup, which

provided a better amplification of the QMS signal in UHV.

4.2.4 VACUUM CHAMBERS - SETUP

In the first setup 3 chambers were mounted, where in the first stage the gas emerging from the nozzle was shot in the direction of a skimmer with a diameter of 500 μm. The first formation of the beam took place here. After this formation the gas jet still had to fly through a second slit with a diameter of 2 mm, which was meant to further reduce the background signal coming from the not directed part of the beam. In the last chamber the reaching atoms and molecules could then be analyzed with a QMS system. In figure 4.12 a drawing of the vacuum chambers can be seen.
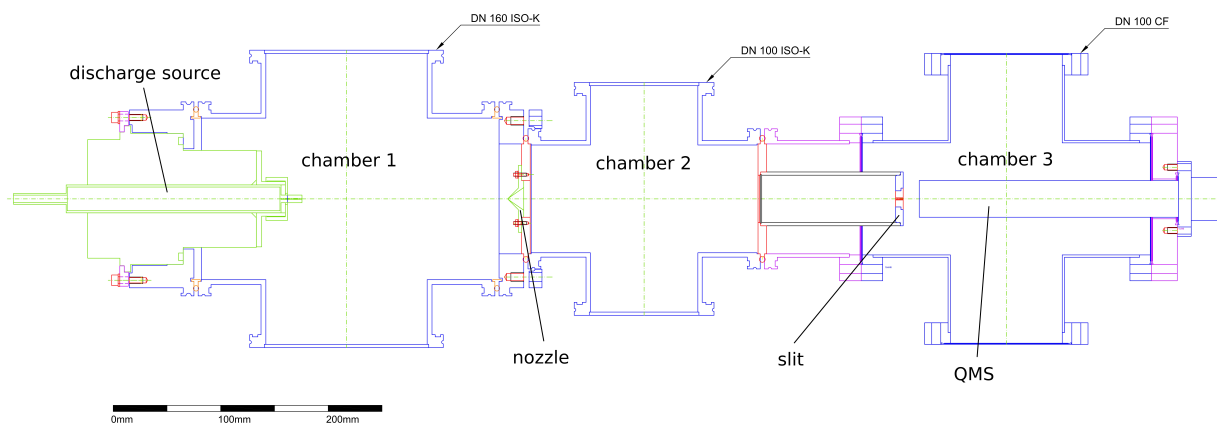
Figure 4.12: Drawing of the vacuum chambers. Hydrogen is dissociated in the green part on the very left side, shoots on the skimmer ($\varnothing$ 500 μm), where only the directed part can enter the second chamber. The beam shoots into the cylindrical tube, where at the end caps, formed of teflon, a hole with a diameter of 2 mm functions as a slit. Only the not diverging part of the beam can enter the last chamber where a QMS is mounted and analyzes the beam.

In these chambers three turbo molecular pumps (TMP) plus backing pumps produced the vacuum. The pumping system for the first chamber consisted of:

- chamber 1:
  backing pump: Varian SD 700;
  TMP: Leybold Oerlikon Turbovac 361 (iso-K 160)

- chamber 2:
  backing pump: Leybold oilfree scroll vacuum pump SC 15 D;
  TMP: Leybold Oerlikon Turbovac TW 250 S (iso-K 100)

- chamber 3:

  backing pump: Leybold oilfree scroll vacuum pump SC 15 D;

  TMP: Pfeiffer TMU 261 (CF 100)

The TMPs at chamber 2 and 3 shared the scroll pump SC 15 D together as a backing pump.
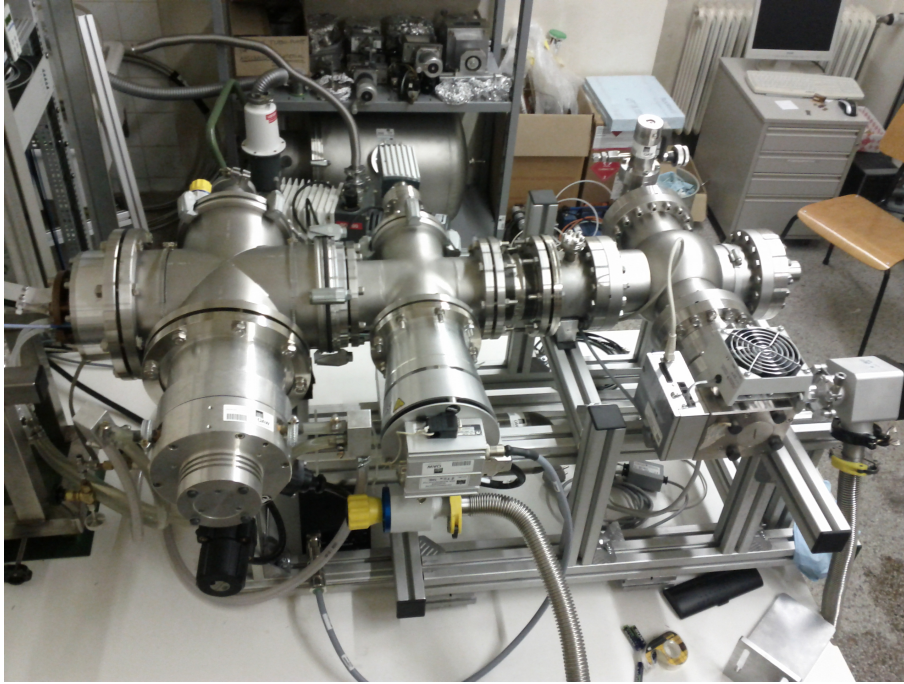
Figure 4.13: Picture of the vacuum system.

A Balzers IKR 020 for low pressure and Balzers TPR 010 for high pressure measurement showed the pressure in chamber 1 and two Leybold ITR 90, each mounted at chamber 2 and 3, measured the pressure there.

A straight line from the source through the skimmer and slits was obligatory for a maximum of the beam to reach the last chamber. Hence a good calibration of the whole setup had to be done (even though the beam divergence in the first chamber should be quite huge). This justification was reached with a laser shooting through the aperture.

The search for leaks in the vacuum system was done with a helium leak detector (Pfeiffer smart test HLT 570). With this method even very small leaks could be found. After leak detection and some days of pumping, pressure in the chambers reached ultra high vacuum (UHV). In chamber 1 total pressure was in the order of middle 10^{-8} mbar, chamber two leveled off at deep 10^{-7} mbar and chamber three reached the deep 10^{-9} mbar region (minimum pressure 2.6×10^{-9} mbar).
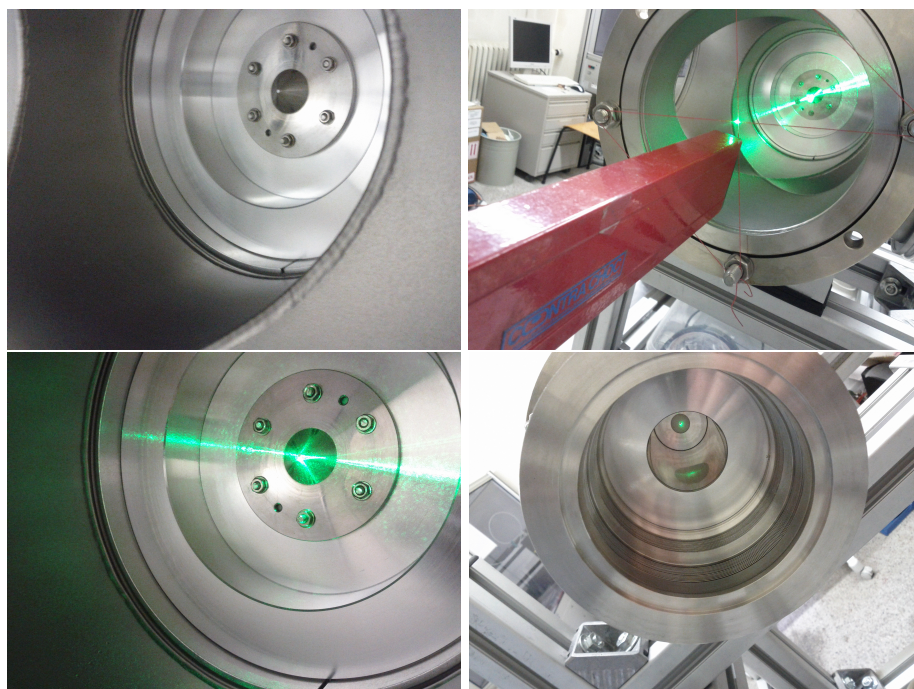
Figure 4.14: Pictures of the laser alignment.

4.2.5 RESULT

For the first test of this setup a tube made of aluminum and later teflon was put on the nose of the glass tube, to lead the gas coming out of the capillary onto the skimmer. It was meant that a bigger amount of hydrogen would fly through the skimmer and form a more dense gas beam. With a gas flow through the glass tube a signal was detected in the last chamber, which could be interpreted as a incoming hydrogen gas beam (see figure 4.15 with partial pressures of mass 1 and mass 2).

When gas was turned on the total pressures in the chambers were: $p_{chamber1}$: 8×10^{-6} mbar, $p_{chamber2}$: 1.39×10^{-6} mbar and $p_{chamber3}$: 2.8×10^{-8} mbar. (background pressure p_{ch3}: 8.9×10^{-9} mbar) Furthermore the pressure in the hydrogen supply pipe $p_{H_2 supply}$ was 0.463 mbar. A correlation of of the pressures in the chambers can be seen in figure 4.16 and 4.17

Different papers say that for the same gasflow, when the microwave discharge source is turned on, the pressure in the gas system is higher than when the discharge source is turned off (e.g. [21]). We could confirm this behavior. This result can be interpreted as such, that the microwaves heat the gas, which therefore increases the pressure in the gas system. See figure 4.18 for the different pressures with same gas flow when the source was turned on/off.
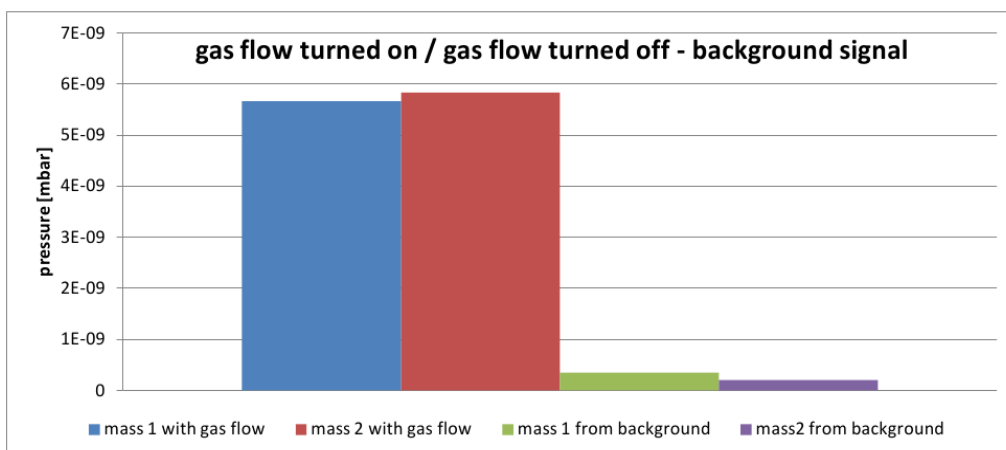
Figure 4.15: left two bars show the partial pressures measured with the QMS when hydrogen flow was turned on. The right two bars show the pressure when no beam was there - the background signal
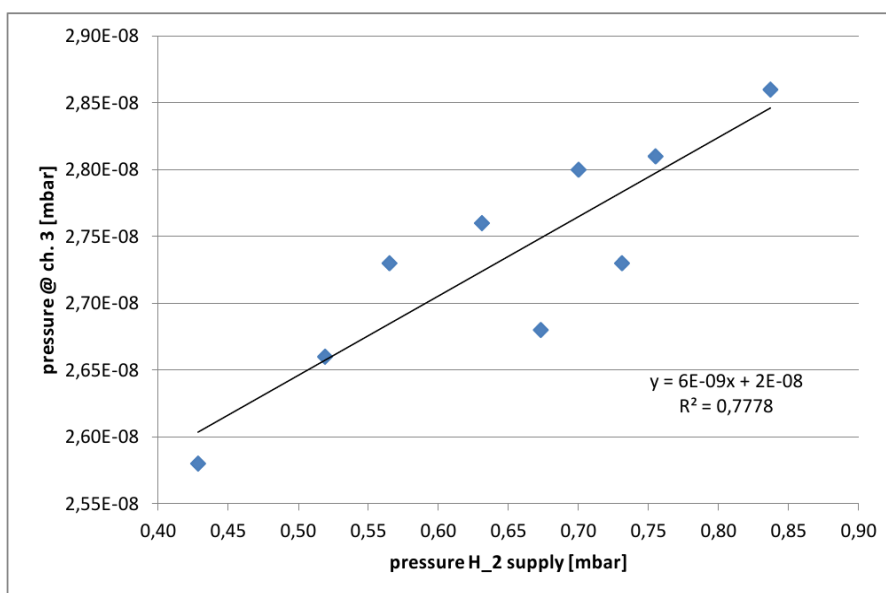
Figure 4.16: Correlation of pressure increase in chamber 3 with hydrogen supply pressure.

Regarding hydrogen dissociation the tests did not show any significant result as seen e.g. in figure 4.19 (Tests with the teflon tube instead of aluminum on the nose of the glass tube had also shown no significant increase in mass 1.)

Therefore the next try in searching for hydrogen dissociation was to do measurements without a tube on the source. Unfortunately these tests did not show a bigger amount in mass 1, but we could see that a beam arrived in the chamber without a tube on the dissociation source (see figure 4.20 and 4.21).
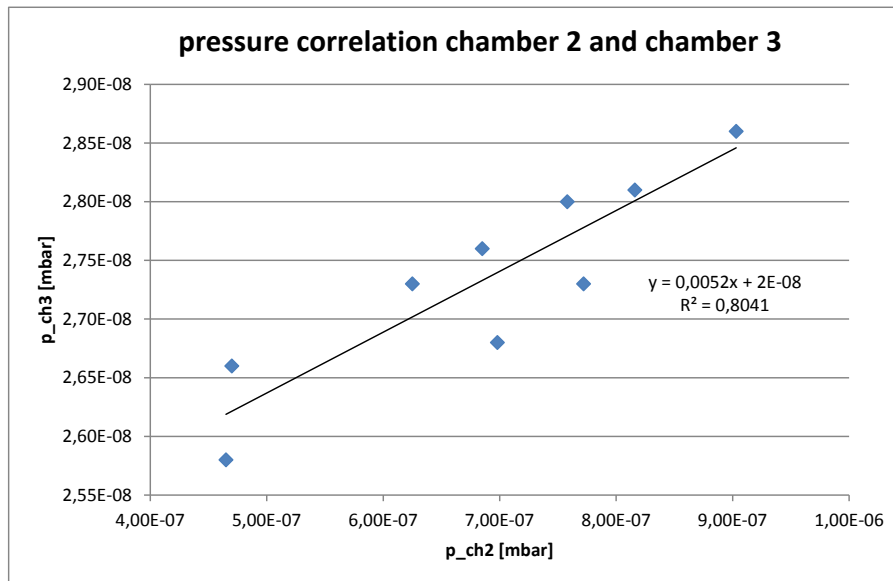
Figure 4.17: Correlation of pressure chamber 2 and chamber 3 when there was a gas flow.
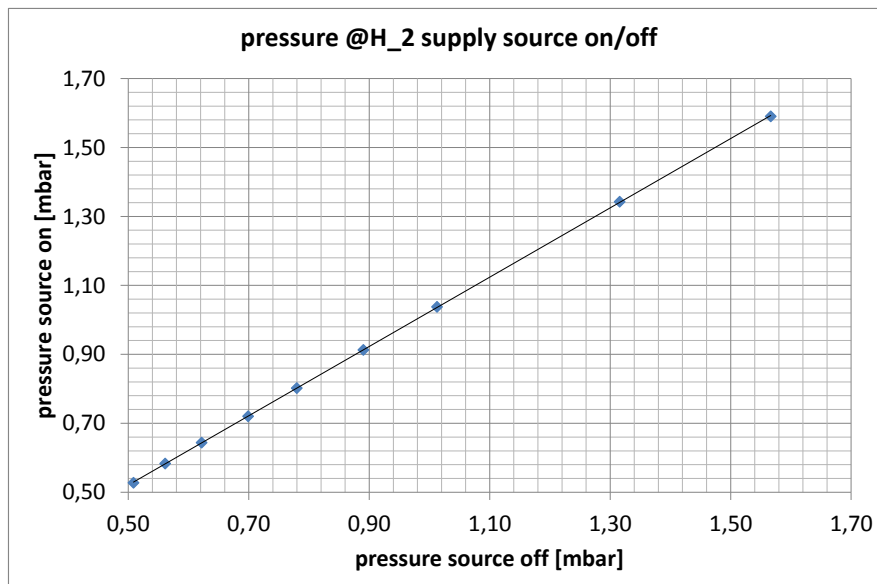
Figure 4.18: Different feed pressures, microwave source turned on/off. Pressure in the gas system increased a little bit because the of heating by the microwaves.
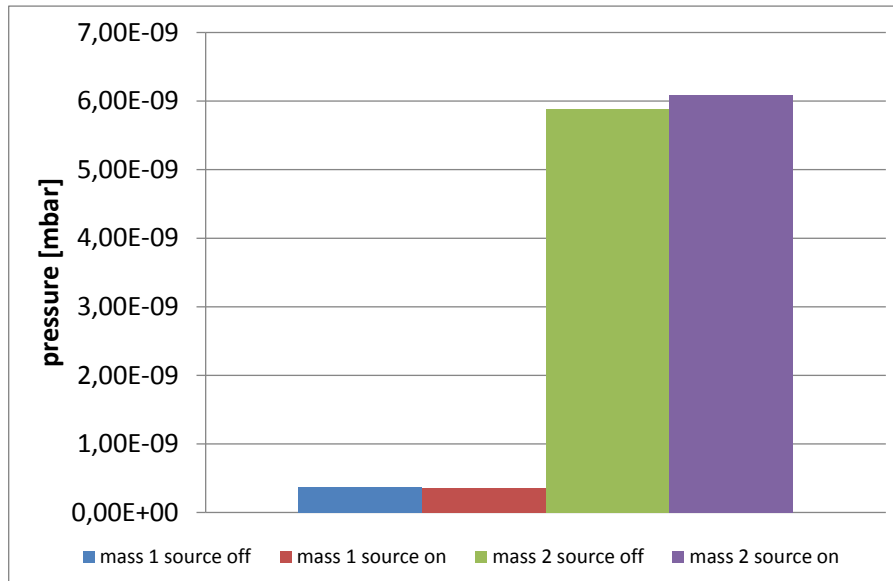
Figure 4.19: dissociation source turned on and off (with teflon tube). No significant production of mass 1 can be observed. mw-power $= 30\%$, refl. mw-power$= 11\%$, $p_{H_2 supply} = 0.72$ mbar, $p_{ch1} = 1.2 \times 10^{-5}$ mbar, $p_{ch2} = 2.44 \times 10^{-6}$ mbar, $p_{ch3} = 2.75 \times 10^{-8}$ mbar

The conclusion of this experiment was, that there were two background parts. The one was a result of the hydrogen recombination in the last chamber. The other signal came from the residual water vapor, which should be reduced in the next steps. Because of the measurements (also estimations with the assumption that the beam coming out of the source diverges very strong, typical opening angle 60°) we came to realize that at least the background signal in the last chamber had to be reduced of about one order of magnitude. At the same time one chamber should also be added in the very first part of the vacuum system, so that all the diverging parts of the beam would not reach the last chamber and thus increase background signal in mass 1 and 2.
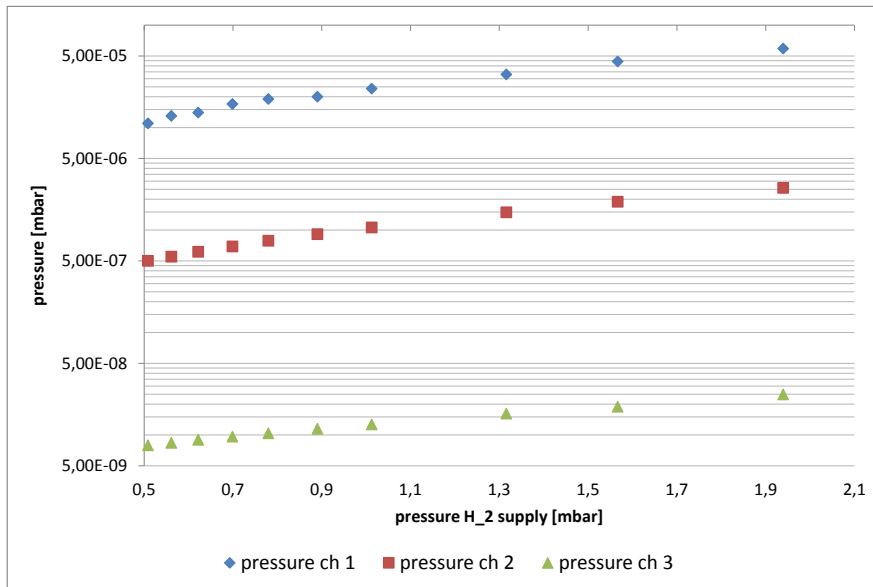
Figure 4.20: pressure at the vacuum chambers as a function of supply pressure.
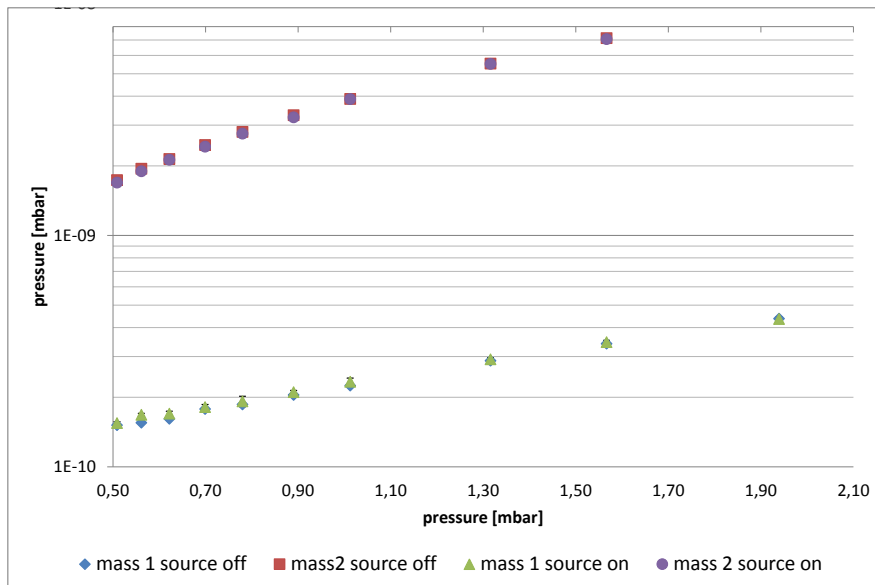
Figure 4.21: Pressure at chamber 3 as a function of supply pressure, dissociation source turned on and off, no tube on the source, no significant production of mass 1 can be observed, mw-power $= 30\%$

4.3 FINAL SETUP

As said the main problem of the first setup was the very big background signal in the last chamber. Therefore we added a chamber directly after the source. Our workshop attached a wall in the vacuum flange $45°$ diagonally as can be seen in figure 4.23. In the middle of this wall a teflon plate with a small hole inside ($\varnothing$ 5 mm) was attached. On the new "chamber" a oil diffusion pump (Leybold DIP 3000) with a pumping speed of 3000 l/s was installed.
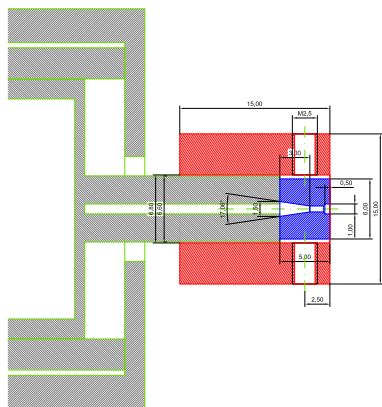
Figure 4.22: Schematic drawing of the teflon nozzle.

In this chamber the pump evacuated the diverging part of the beam. Only the directed part was able to enter through the slit in the wall into the following chamber, through the skimmer and finally through the last slit into the detection chamber. A laval type nozzle (teflon, $\varnothing 600 \ \mu$m, crafted by our workshop) was installed on the nose of the source for an efficient formation of the beam (4.22).
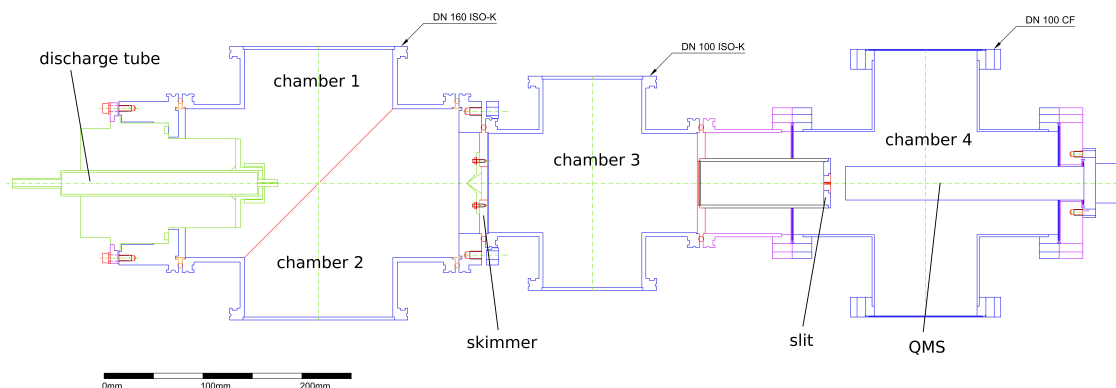
Figure 4.23: Schematic drawing of the final setup.

Many methods then were tried to reduce the pressure in the 4th chamber (the detection chamber) for a reduction of the background signal. First we mounted an ion getter pump (Varian Vaclon Plus 20 - Star Cell) which in theory should have a ultimate pressure below 10^{-11} mbar. The Balzers IKR 020 and TPR 010 measured the pressure in chamber 1. In chamber 3 and 4 Leybold ITR 90 gauges measured the pressure. After a couple of days of pumping and baking out for 24 hours at $200°$ the ion getter pump did not reach the desired

pressure, it did not even reach the pressure from the first setup in the detection chamber.

Figure 4.24: Picture of the whole setup.

Hence we installed a small turbo molecular pump Leybold Turbovac 50 on the Pfeiffer TMP to reduce the back drift of hydrogen into the detection chamber. Then the ion getter pump was swapped with an old getter pump (SAES getters Sorb AC C 200-MK5-100 ST-707). Reactivation of this pump did not work, which meant that the getter material was dead. A new getter material was ordered. Since the delivery would take a couple of weeks for the time being we tested other pumping systems.

4.3.1 FIRST HINTS

The next step was the replacement of the getter pump. A self made cryopump was installed, which consisted of little carbon sticks glued on a aluminum plate, which again was attached to a helium cold head (APD cryogenics HC-4 MK1). Also the QMS system was changed vs. a Pfeiffer Prisma (QME200/QMA200 a plot of the linearity can be seen in the appendix). This QMS had a more open ionization source, which was meant to reduce the possibilities

of recombination. In this tests the vacuum system reached a base pressure of 6.8×10^{-9} mbar, which was still worse than in the tests without any further pump installed at the detection chamber. Also a big amount of carbon compounds could be observed (which was not a problem for the measurement of mass 1 and 2).
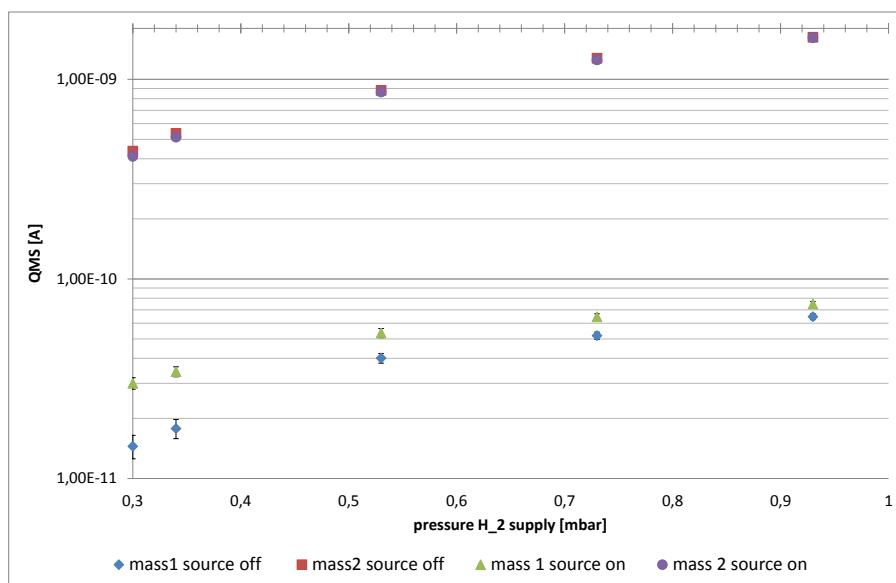
Figure 4.25: Tests with the cryopump installed. As can be seen when the source is turned on, a bigger amount of mass 1 is detected (the plot is already background reduced).

CROSSCHECK

We did some crosschecks with helium gas to confirm that a gas beam was formed. The Helium gas was introduced through the glass tube. In this arrangement minimum base pressure was 2.6×10^{-9} mbar. Results can be seen in figure 4.26

4.3.2 FINAL RESULTS

As seen in the last results there was a very small signal difference in ionized molecules done by the QMS and hydrogen atoms coming from the source. Still the main problems were the very big background signal and the recombination of the atoms. In this last change of the setup we installed a new getter material on the getter pump used before, and mounted the pump on the detection chamber. With this pumping system a pressure of
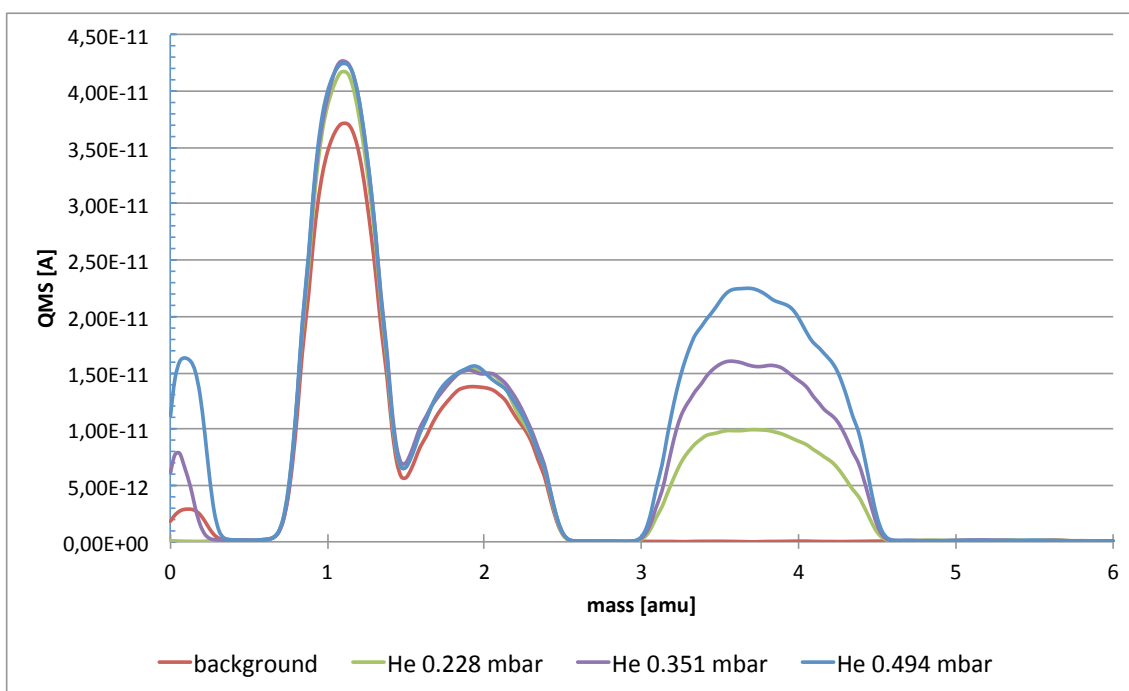
Figure 4.26: Crosscheck of the gas beam with Helium. Helium gas was shot through the source and then detected with the QMS. It can be observed, that mass 4 rises with more gas flow through the source.

less than 5×10^{-10} mbar was reached after a short period (signal was out of range of the pressure gauges).

Further tests were done to confirm that the beam reaches the last chamber. The method was to form a beam from the source, measure the pressure rising in chamber 3 (chamber before detection), then introduce hydrogen there reaching the same pressure and compare the signal detected by the QMS (hydrogen introduced with a inlet valve). Base pressure in chamber 3 was 1.26×10^{-8} mbar. With a pressure in the hydrogen supply of 2.26 mbar the pressure in chamber 3 reached 1.68×10^{-8} mbar. When hydrogen was introduced into this chamber until the desired pressure, the signal at the QMS was far more smaller than the signal resulting from the hydrogen supply (see figure 4.27). Hence the formation of a gas beam was confirmed.

Finally we measured the dissociation of hydrogen again with a microwave power of 30% and 40%. As can be seen in the plots the with a mw-power of 40% dissociation is a bit better. Also the more gas flow through the pyrex tube the less dissociation can be observed. The degree of dissociation D was calculated with the formula given by McCullough et al. [18]:
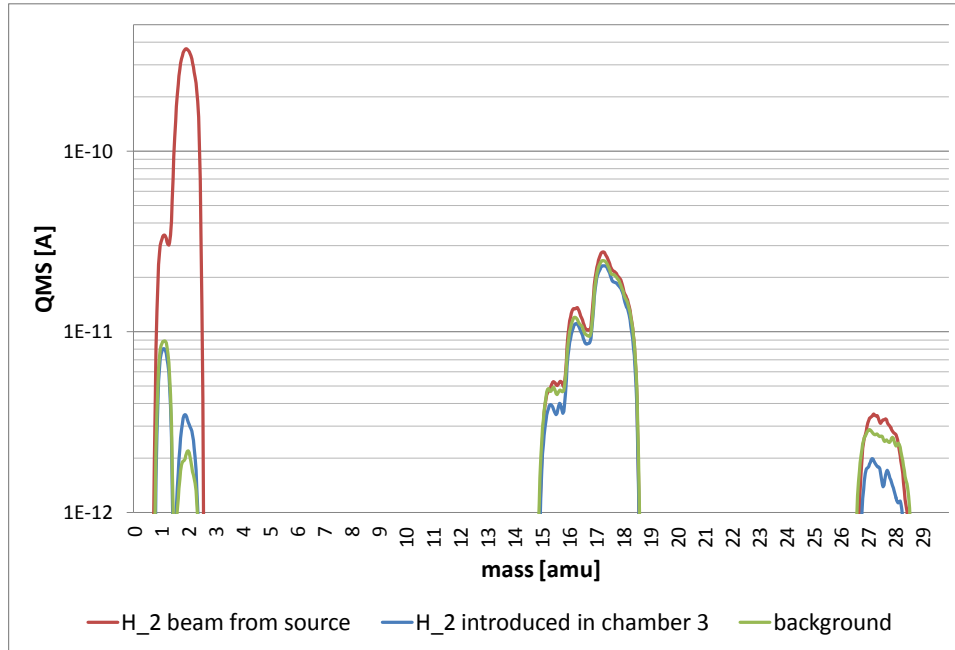
Figure 4.27: Crosscheck of the gas beam. Signal detected in chamber 4 with the QMS. The background in chamber 3: $p_{ch3} = 1.26 \times 10^{-8}$ mbar; pressure when hydrogen was introduced into chamber 3: $p_{ch3} = 1.68 \times 10^{-8}$ mbar; pressure in chamber 3 when gas was introduced as hydrogen beam (from source): $p_{ch3} = 1.68 \times 10^{-8}$ mbar;

$$D = (S_1 - S_2)/S_1 \qquad (4.2)$$

where S_1 is the molecular Signal with dissociation turned off, S_2 the corresponding molecular Signal, when source is turned on and D the dissociation fraction.

In this measurement we were able to successfully observe a H_1-beam 1 meter from the nozzle!
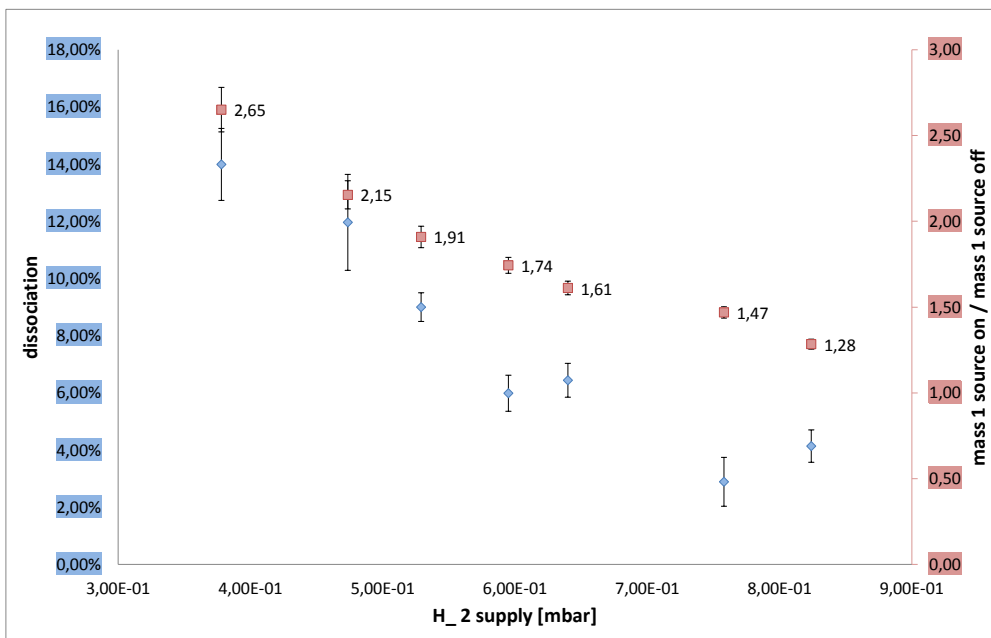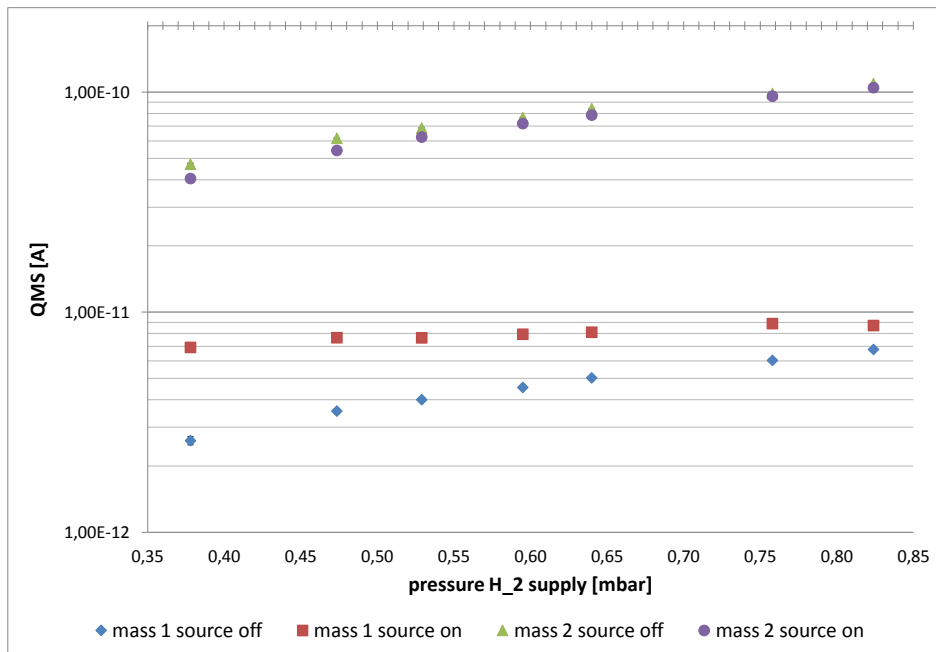
Figure 4.28: Measured dissociation (background reduced) with 40 % microwave power. The formula that yields the dissociation factor was given by McCullough et al. as $D = (S_1 - S_2)/S_1$.
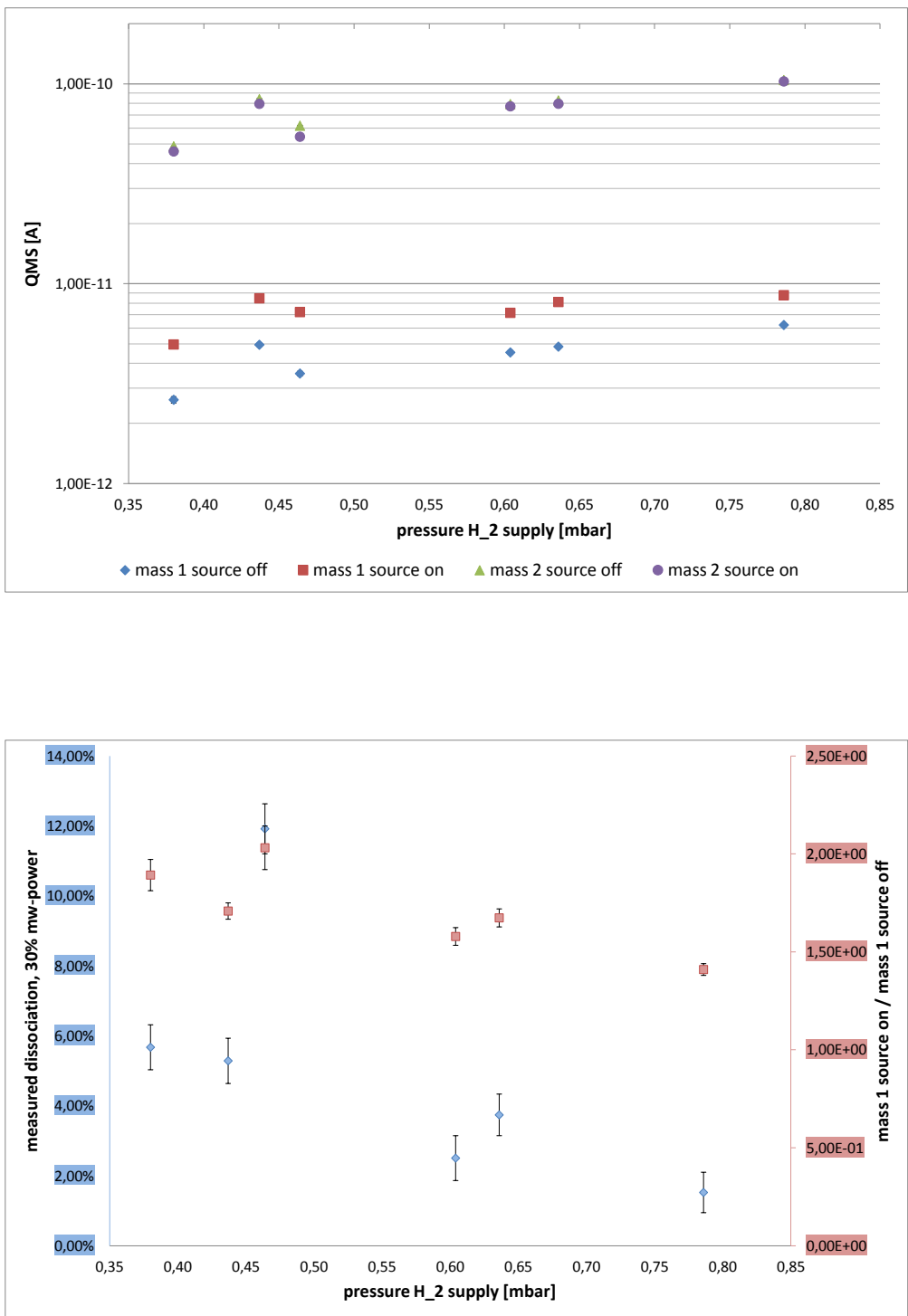
Figure 4.29: Measured dissociation (background reduced) with 30 % microwave power. The formula that yields the dissociation factor was given by McCullough et al. as $D = (S_1 - S_2)/S_1$.

Values for 40 % microwave power

pressure H_2 supply [mbar]	$(H_{2off}-H_{2on})/H_{2off}$	ERROR	mass1 source off	ERROR	mass1 source on	ERROR	m1_source_off/ m1_source_on	ERROR
0,378	13,99%	1,26%	2,60959E-12	1,112E-13	6,91735E-12	1,67E-13	2,65074373	0,1299
0,4736	11,96%	1,68%	3,5555E-12	9,151E-14	7,65881E-12	2,15E-13	2,154074775	0,0821
0,529	9,00%	0,50%	4,00635E-12	9,554E-14	7,64757E-12	1,73E-13	1,908862667	0,0627
0,595	5,99%	0,63%	4,55415E-12	9,277E-14	7,94019E-12	1,36E-13	1,743505531	0,0464
0,64	6,44%	0,59%	5,03211E-12	9,899E-14	8,10927E-12	1,22E-13	1,611503996	0,04
0,758	2,89%	0,85%	6,04164E-12	1,082E-13	8,87496E-12	1,18E-13	1,468964829	0,0327
0,824	4,14%	0,56%	6,7726E-12	1,155E-13	8,69736E-12	1,29E-13	1,28419778	0,029

Values for 30 % microwave power

pressure H_2 supply [mbar]	$(H_{2off}-H_{2on})/H_{2off}$	ERROR	mass1 source off	ERROR	mass1 source on	ERROR	m1_source_on/ m1_source_off	ERROR
0,464	11,92%	0,72%	3,55116E-12	9,779E-14	7,21324E-12	3,42E-13	2,031236426	0,1115
0,437	5,29%	0,65%	4,94824E-12	9,707E-14	8,45304E-12	1,23E-13	1,708293638	0,0417
			8,41972E-12	1,241E-13	1,16664E-11	1,08E-13	1,385598947	0,0241
0,636	3,74%	0,59%	4,84185E-12	9,578E-14	8,10304E-12	1,54E-13	1,673542088	0,0459
0,786	1,52%	0,58%	6,21528E-12	9,482E-14	8,76256E-12	1,3E-13	1,409841985	0,03
0,604	2,50%	0,64%	4,53009E-12	1,028E-13	7,15081E-12	1,23E-13	1,578515726	0,045
0,38	5,67%	0,64%	2,62465E-12	9,687E-14	4,96582E-12	1E-13	1,891991178	0,0796

Table 4.1: Measured values of dissociation of hydrogen, mass 1 when the dissociation source was turned off and on and the ratio of mass 1 with the dissociation source turned off and mass 1 with the dissociation source on for 30 % and 40 % microwave power.

CHAPTER 5

DISCUSSION AND OUTLOOK

5.1 DISCUSSION

In our setup we were able to produce a directed beam and detect this beam with a QMS. We have clearly seen a signal downstream when gas was introduced into the vacuum system. Therefore the differentially pumped vacuum system stood the test.

The production of hydrogen induced by a microwave system could also be seen, although the measured value of dissociation was somehow less than expected. The highest measured value of dissociation was about 14 % for 40 % microwave power. As discussed earlier, this value was measured with a gasflow, where the discharge tube had the best working point (see figure 3.7, pressure at H_2 supply approximately 0.4 mbar). With a higher gasflow (pressure at H_2 supply approximately 0.8 mbar) the measured degree of dissociation reduces to zero.

For 30 % microwave power the dissociation source behaves quite similar with the difference that the highest measured degree of dissociation is 12 %.

The dissociation source which produced our hydrogen beam was already used by a group of Aarhus University. They reported a dissociation fraction in the order of 90 %, but their detection method was different and they measured the signal of the beam just a few centimeters away from the source. There could be many reasons why the value of dissociation was lower in our setup.

The first problem was the detection. As mentioned we used a Pfeiffer Prisma QMS with an opened ionization source. Here the problem is that it is not really possible to shoot directly into the QMS. Thus many of the atoms which reach this point recombine when they hit the wall or the ionization source. Another problem about the mass spectrometer

is that it is very slow and therefore no background reducing methods could be applied. Also a problem could be even more upstream e.g. that the hydrogen we used was not clean enough. For the next step we plan to use ultra-pure hydrogen cleaned with a palladium filter

In summary the monoatomic hydrogen beam setup worked fine and we were able to clearify the items which have to be improved.

5.2 OUTLOOK

In the next stage of this experiment it will be tried to gain a better control of the beam parameters. We have clear identified the items to be improved: A new QMS with a crossed beam ionization source will be used instead of the ones used until now. In order to use background reducing techniques this mass spectrometer will be read out in another way. A chopper will then modulate the beam sinusoidally. With the frequency of the chopper and the signal in the QMS it will be possible to use phase sensitive techniques like a lock-in amplifier.

An improvement of the gas system will also be applied. Instead of the hydrogen gas tank a hydrogen dissociation machine will be used which will produce hydrogen gas due to electrolysis out of water. This machine has a palladium filter which will make ultra-pure hydrogen. Also the inlet valve will be exchanged vs. a new flowmeter (mainly because the inlet valve had a drift and the flow always had to be adjusted by hand).

Once the whole production of mass 1 will work properly, the next steps will: be cool the beam to e.g 50 K, polarize the beam with sextupoles, and do the whole Rabi like experiment at the CERN facility.

Appendices

TE MODES

(from Demtröder - Experimentalphysik2) For a cuboid with edge lengths a, b, c and ideal guiding walls the E-field $\vec{E} = (E_x, E_y, E_z)$ has the boundary condition, that the tangential components at the wall equals zero. This means:

- $E_x = 0$ for $z = 0, c$ and $y = 0, b$;

- $E_y = 0$ for $x = 0, a$ and $z = 0, c$;

- $E_z = 0$ for $x = 0, a$ and $y = 0, b$;

When an electromagnetic wave with a wave vector $\vec{k} = (k_x, k_y, k_z)$ is produced in the cavity, the wave is reflected at the walls. There will be a stationary standing wave when the boundary condition is

$$k_x = \frac{n\pi}{a}; \quad k_y = \frac{m\pi}{b}; \quad k_x = \frac{q\pi}{c}; \tag{.1}$$

with $n, m, q \in \mathbb{N}$. Because

$$|\vec{k}| = \sqrt{k_x^2 + k_y^2 + k_z^2} \tag{.2}$$

.1 becomes

$$|\vec{k}| = k = \pi\sqrt{\frac{n^2}{a^2} + \frac{m^2}{b^2} + \frac{q^2}{c^2}} \tag{.3}$$

For the possible frequencies ω of a standing wave with $\omega = c_0 k$ (c_0 velocity of light in the vacuum)

$$\omega = c_0\pi\sqrt{\frac{n^2}{a^2} + \frac{m^2}{b^2} + \frac{q^2}{c^2}} \tag{.4}$$

is obtained. Thus in a cuboid only standing waves of the form

$$\vec{E}_{n,m,q} = \vec{E}_0(n, m, q) \cos \omega t$$

are possible, where $\vec{E}_0 = (E_{0x}, E_{0y}, E_{0z})$ and

$$E_{0x} = A \cos \frac{\pi n}{a} x \sin \frac{\pi m}{b} y \sin \frac{\pi q}{c} z$$
$$E_{0y} = A \sin \frac{\pi n}{a} x \cos \frac{\pi m}{b} y \sin \frac{\pi q}{c} z$$
$$E_{0x} = A \sin \frac{\pi n}{a} x \sin \frac{\pi m}{b} y \cos \frac{\pi q}{c} z \qquad (.5)$$

The field amplitude E_{01} is standing vertical on the wave vector k. This ideal guiding cuboid is called cavity resonator and the standing waves .5 resonator modes.

If the electric vector is perpendicular to the direction of propagation, ($\vec{E}_0 = (E_{0x}, E_{0y}, 0)$) then the waves are called TE-waves (transverse-electric)[7].

QMS

A QMS (quadrupole mass spectrometer) consists of an ionization source, which ionizes neutral atoms, four parallel rods which build the filter system of the mass spectrometer and a detector. Between two rods a voltage like in figure .1

$$U_1 = U + V \cos \omega t \qquad (.6)$$

is applied (U_1 used voltage, U applied DC voltage, V applied AC Voltage, ω angular frequency, t time). Only particles with a certain ratio of mass to charge will then pass through the rod system. Finally the ions, which are passing are detected by a faraday cup or a channel electron multiplier.

The ionization source of the Pfeiffer looked like in figure .2

[2]
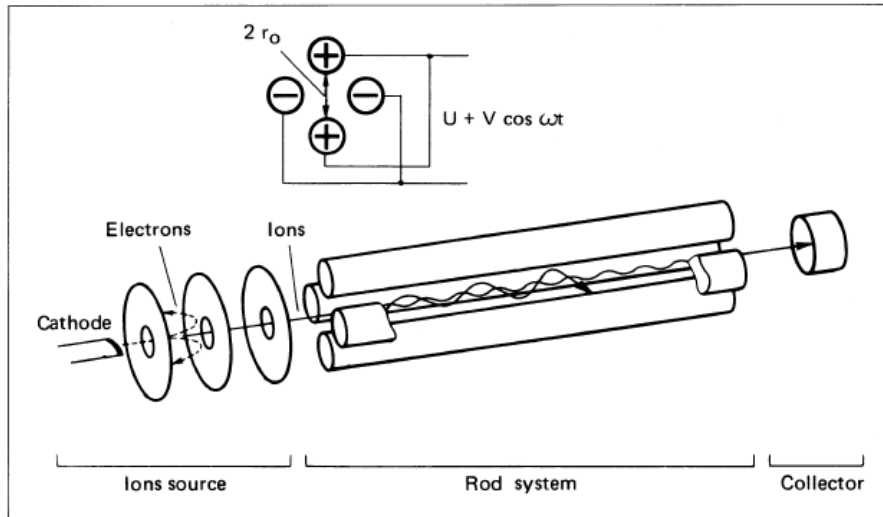
Figure .1: Schematic view of a QMS system. Neutral atoms are ionized at the ionization source. In the rod system only a certain part of mass to charge ratio will pass. Then positively charged ions, which are passing are detected in a faraday cup or a channel electron multiplier.

Figure .2: Open Ionization source of the Pfeiffer QMS.
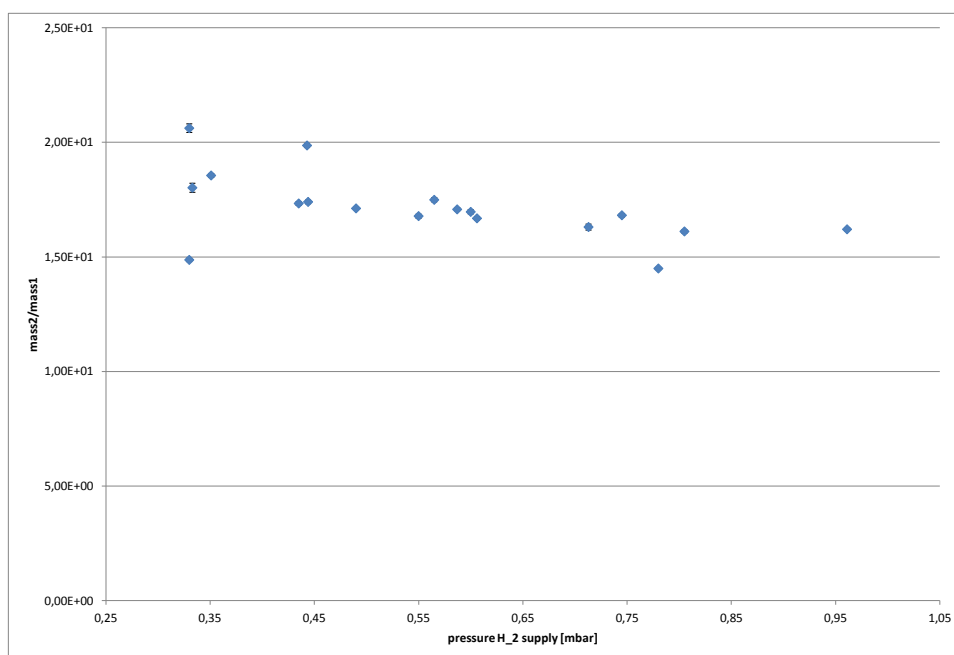
Figure .3: Linearity of the amplification of the Pfeiffer QMA 200 QMS electron multiplier (from different data)

LABVIEW PROGRAM
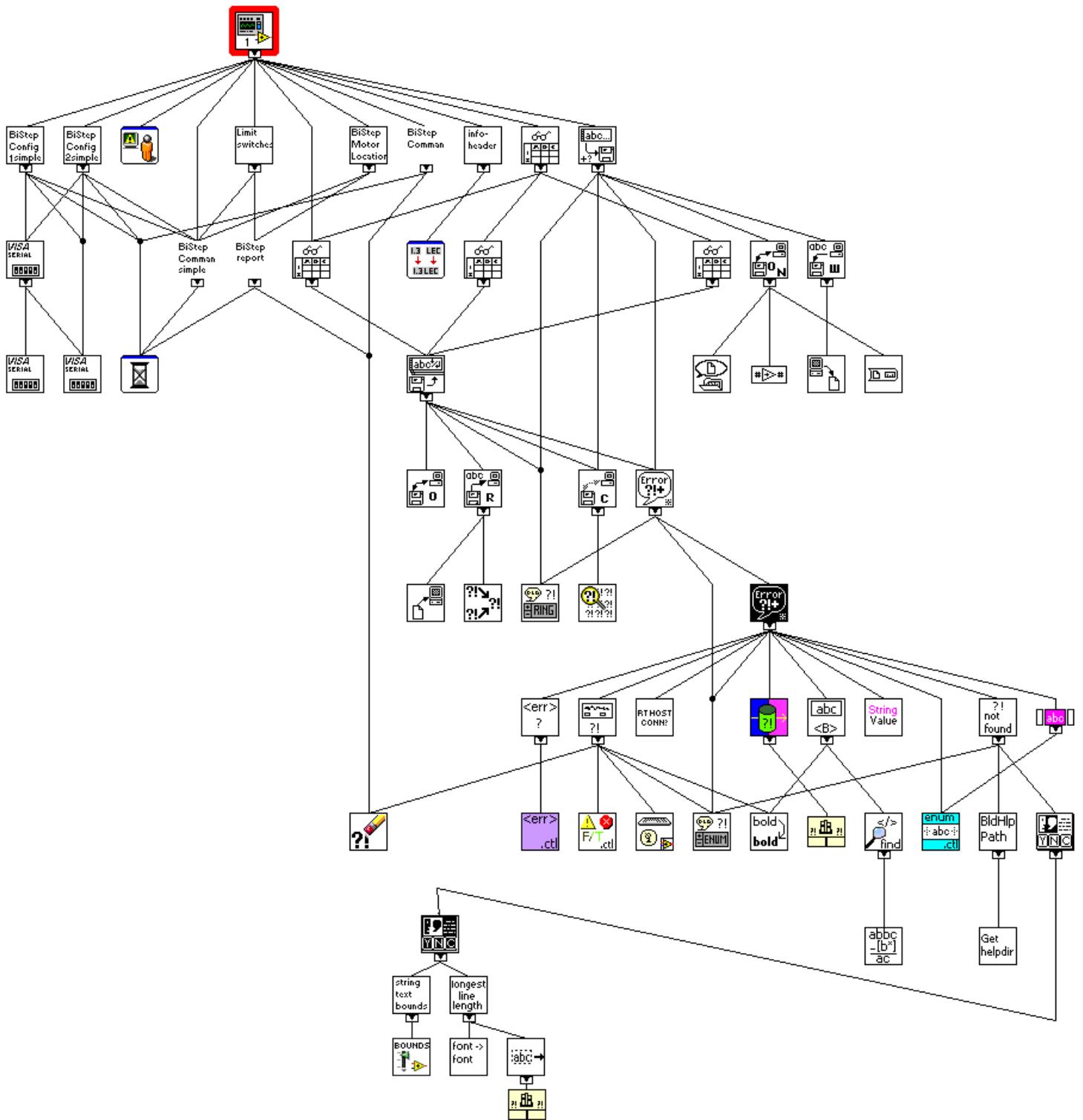
Figure .4: LabView program for controlling the bi-step motors

INSTRUMENTS

SOURCE

- Microwave generator: Muegge - MW-GPRYJ1511-300-01, 300 W, 2.45 GHZ

- Tesla spark: Goodburn Engeneering - HV spark tester model E1/D, 240 V

GAS SYSTEM

- OMEGA FMA-1904-N2 flowmeter

- Needle Valve: balzers UDV 040

- Pressure gauges: Leybold CTR 90, A-Net Crystal gauge, Keller AG PAA 23 (0-20 bar, read out by GIA 1000 NS), Keller AG PAA-21-10 (0-10 bar read out by GIA 1000 NS)

- diaphragm pump: Pfeiffer MVP 055-3,

VACUUM

NOZZLE TESTING

- Leybold TRIVAC B S65B

- Leybold RUVAC WAU 501

- Pressure gauge: Leybold Ceravac CTR90

VACUUM SETUP

- TMP: Leybold Oerlikon Turbovac 361, Leybold Oerlikon Turbovac TW 250 S, Pfeiffer TMU 261, Leybold Turbovac 50

- Backing pumps: Varian SD 700, Leybold oilfree scroll vacuum pump SC 15 D, Alcatel 2033

- Oil diffusion pump: Leybold DIP 3000

- Ion getter pump: Varian Vaclon Plus 20 - Star Cell

- Getter pump: SAES SORB-AC C 200-MK5-100 ST-707

- Kryo pump: Stefan-Meyer productions

- Pressure gauges: Leybold ITR 90 (read out by Center Three), Balzers IKR 020, TPR 010

- All-metal inlet valve: UDV 040

- Helium leak detector: Pfeiffer smart test HLT 570

- QMS: Spectra (MKS), Pfeiffer QME 200/QMA 200

BIBLIOGRAPHY

[1] B. Koch: *A comment on the opera result and cpt*. arXiv 1109.5721v3 (2011)

[2] Pfeiffer Vacuum GmbH: *Vacuum Technology Know How*. Pfeiffer Vacuum GmbH (2009)

[3] K. Blaum, F. Herfurth: *Trapped Charged Particles and Fundamental Interactions*, chap. Fundamental Tests with Trapped Antiprotons, 155–188. Springer, lect. notes phys. edn. (2008). ISBN 978-3-540-77816-5

[4] J. W. Cronin: *The experimental discovery of cp violation*. Lect. Notes Phys. **764**, 261–280 (2008)

[5] R. S. Hayano, M. Hori, D. Horvath, E. Widmann: *Antiprotonic helium and cpt invariance*. Rep. Prog. Phys. **70**, 1995–2065 (2007)

[6] A. collaboration: *Atomic spectroscopy and collisions using slow antiprotons*. CERN-SPSC **2005-002** (2005)

[7] W. Demtröder: *Experimentalphysik 2 - Elektrizität und Optik*. Springer-Lehrbuch, 3rd edn. (2004). ISBN 3-540-20210-2

[8] H. Haken, H. C. Wolf: *Atom- und Quantenphysik*. Springer-Lehrbuch (2004). ISBN 3540026215

[9] T. Fließbach: *Mechanik - Lehrbuch zur Theoretischen Physik I*. Spektrum-Lehrbuch, 4th edn. (2003). ISBN 3-8274-1433-4

[10] E. te Sligte, R. C. M. Bosch, B. Smeets, P. van der Straten, H. C. W. Beijerinck, K. A. H. van Leeuwen: *Magnetic nanodots from atomic fe: Can it be done?* PNAS (2002)

[11] J. Eades, F. J. Hartmann: *Forty years of antiprotons*. Review of Modern Physics **71** (1999)

[12] N. Koch, E. Steffens: *High intensity source for cold atomic hydrogen and deuterium beams*. Rev. Sci. Instrum. **71/3**, 1631 (1999)

[13] D. Colladay, V. A. Kostelecky: *Lorentz-violating extansion of the standard model*. Phys. Rev. D **58**, 116002 (1998)

[14] D. Colladay, V. A. Kostelecky: *Cpt violation and the standard model*. Phys. Rev. D **55**, 6760 (1997)

[15] Peskin, Schroeder: *An Introduction to Quantum Field Theory*. Perseus Books (1997). ISBN 978-0201503975

[16] E. Leader, E. Predazzi: *An introduction to gauge theories and modern particle physics vol. 2*. Camridge Monographs on Particle Physics, Nuclear Physics and Cosmology (1996). ISBN 0-521-49617-9

[17] F. Werner, D. Kozec, J. Engemann: *Slot antenna 2.45 ghz microwave plasma source*. Plasma Sources Sci. Technol. **3**, 473–481 (1994)

[18] R. W. McCullough, J. Geddes, A. Donnelly, M. Liehr, H. B. Gilbody: *A new reactive atom beam source for accelerator target studies*. NIM B **B79**, 708–710 (1993)

[19] A. Donnelly, M. P. Hughes, J. Geddes, H. B. Gilbody: *A microwave discharge atom beam source of high intensity*. Meas. Sci. Technol. **3**, 528–532 (1992)

[20] Y. Suetsugu, Y. Kawai: *Rf field in a slotted-type lisitano coil*. Jap. Journal of Appl. Phys. **23/8**, 1101–1106 (1984)

[21] J. T. M. Walraven, I. F. Silvera: *Helium-temperauture beam source of atomic hydrogen*. Rev. Sci. Instrum. **53/8**, 1167 (1982)

[22] O. F. Hagena, W. Obert: *Cluster Formation in Expanding Supersonic Jets: Effect of Pressure, Temperature, Nozzle Size, and Test Gas*. J. Chem. Phys. **56**, 1793 (1972)

[23] H. Wise, B. J. Wood: *Reactive collisions between gas and surface atoms*. Advances in Atomic and Molecular Physics **3**, 291–353 (1968)

[24] J. B. Anderson, J. B. Fenn: *Velocity distribution in molecular beams from nozzle sources*. The Physics of Fluids **8/5**, 780 (1965)

[25] J. Geddes, R. W. McCullough, A. Donnelly, H. B. Gilbody: *Dissociation of hydrogen in high frequency discharges*. Plasma Sources Sci. Technol. **2**, 93 (1962)

[26] C. C. Goodyear, A. von Engel: *Dissociation and ionization of hydrogen in high frequency discharges*. Proc. Phys. Soc. **79**, 732 (1962)

[27] G. Lüders: *Proof of tcp theorem*. Annals of Physics **2**, 1–15 (1957)

[28] C. S. W. E. Ambler, R. W. Hayward, D. D. Hoppes, R. P. Hudson: *Experimental test of parity conservation in beta decay*. Phys. Rev. **105**, 1413–1415 (1956)

[29] T. D. Lee, C. N. Yang: *Question on parity conservation in weak interactions*. Phys. Rev. **104**, 254–258 (1956)

[30] I. I. Rabi, S. Millman, P. Kusch, J. R. Zacharias: *The molecular beam resonance method for measuring nuclear magnetic moments*. Phys. Rev. **55**, 526–535 (1939)

LIST OF FIGURES

70

Martin Diermaier
Curriculum Vitae, 2012

PERSONAL DATA

Place of birth: Ried im Innkreis, Upper Austria
Citizenship: Austrian
DOB: Nov 15th, 1984

CONTACT INFORMATION

Willing 4
A-4755 Zell an der Pram, Austria
tel.: +43660 / 4950846
email: martin.diermaier@assoc.oeaw.ac.at

EDUCATION

1991-1995 PRIMARY EDUCATION,
Zell an der Pram, Upper Austria

1995-1999 GRAMMER SCHOOL
Gymnasium Schärding, Upper Austria

1999-2003 UPPER HIGH SCHOOL WITH EMPHASIS ON NATURAL
SCIENCES Naturwissenschaftliches Oberstufenrealgymnasium (BORG)
Ried im Innkreis, Upper Austria
Matura (final exam)

2003-2004 CIVIL SERVICE
Institut Hartheim, Upper Austria

2004-2006 DIPLOMA PROGRAMME IN METEOROLOLOGIE AND
GEOPHYSICS, University of Vienna

2006-2012 DIPLOMA PROGRAMME IN PHYSICS,
University of Vienna

2011-2012 DIPLOMA THESIS, Stefan Meyer Institute for Subatomic
Physics (Austrian Academy of Sciences)

LANGUAGES SPOKEN

German – Native
English – excellent fluency, written and spoken.
French – good fluency, written and spoken

SOFTWARE SKILLS

C++, Java, LabView, Matlab
Linux (open suse, Ubuntu, Fedora), Windows XP, Windows 7,
Mac OSX
Office applications, Latex